

RESEARCH ARTICLE

Comparison of very high order (O3–18) flux and Crowley flux, and (O3–17) WENO flux schemes with a 2D nonlinear test problem

Jerry M. Straka¹  | Katharine M. Kanak²  | Paul D. Williams³ 

¹School of Meteorology, University of Oklahoma, Norman, Oklahoma, USA

²Norman, Oklahoma, USA

³Department of Meteorology, University of Reading, Reading, UK

Correspondence

Jerry M. Straka, Prof. Emeritus School of Meteorology, University of Oklahoma, Norman, Oklahoma, USA.

Email: jerrystraka@gmail.com

Abstract

Two-dimensional, nonlinear diffusion-limited colliding plumes simulations were used to demonstrate the improved solution accuracy with very high order O9–18 flux schemes, including upwind-biased and even-centred constant grid flux and Crowley constant grid flux schemes, and odd order weighted essentially non-oscillatory (WENO) flux schemes, along with variations and hybrids of these. All schemes were coupled with comparably high order even-centred Lagrangian interpolations and pressure gradient/divergence approximations, and O18 spatial filtering. Subgrid-scale (SGS) turbulent flux calculations, with a constant eddy-mixing coefficient, were made with O2 spatial approximations (O4–20 accurate SGS turbulent fluxes had little impact). Using a range of resolutions from $\Delta x = \Delta z = 25\text{--}166.66 \dots \text{ m}$ for all schemes comparisons against an O17 flux, 25 m resolution reference solution showed solutions made with $\geq \text{O9}$ fluxes produced (often substantially) improved solutions, both visually and usually objectively, compared to solutions produced with lower order ($< \text{O9}/10$) fluxes, especially at intermediate resolutions (33.33–100 m). Expectedly, odd order solutions were increasingly damped as accuracy was decreased, especially from O9 to O3, especially for WENO solutions, while even order solutions were increasingly contaminated with dispersion and aliasing errors as accuracy was decreased, especially from O10 to O4. Odd order schemes also produced better solutions than even order schemes for $< \text{O9}/10$ fluxes, while the highest order ($\geq \text{O13}/14$) schemes produced the best solutions, for any given resolution. Even order flux and Crowley flux (WENO) solutions were the least (most) computationally expensive, based on either floating-point operations (FPO) or CPU times. Efficient WENO-Sine and proposed hybrid Crowley-WENO(-Sine) schemes required fewer FPOs to produce more accurate solutions than traditional WENO schemes. We are encouraged by the often much improved visual and objective accuracy of very high order ($\geq \text{O9}$) fluxes in simulations of a complex problem, and encourage further testing in numerical weather prediction models.

KEYWORDS

colliding plumes, Crowley, high order numerical approximations, high order upwind and centred fluxes, WENO

1 | INTRODUCTION

Very few studies have considered very high, ninth through to eighteenth, order of accuracy (O9–18; hereafter, O denotes order-of-accuracy), upwind-biased odd order or centred even order advective flux finite difference approximations in the atmospheric sciences, nor have more common \geq O9 flux schemes been compared. To address this, the purpose of this article is to evaluate accuracy and computational cost effectiveness, through visual evaluation and objective error measures, of traditional O3–18 constant grid flux, dimension-split O3–18 constant grid flux Crowley (Crowley, 1968 C68; Smolarkiewicz, 1982 S82; Schlesinger, 1984; Tremback *et al.*, 1987 T87; Bott, 1989; Costa and Sampaio, 1997; Wicker and Skamarock, 2002 WS02; etc.), and O3–17 weighted essentially non-oscillatory (WENO) flux schemes (Jiang and Shu, 1996 JS96; Shu, 1997 S97; Balsara and Shu, 2000 BS00; Shu, 2003 S03; Borges *et al.*, 2008; Gerolymos *et al.*, 2009 G09; etc.) for a slow (e.g. advection and turbulence modes) and fast (e.g. sound and sometimes gravity-buoyancy modes) mode-split system of equations (e.g. Skamarock and Klemp, 1992) using a nonlinear diffusion-limited 2D colliding plumes problem. These types of scheme are chosen as they form a relatively simple basis for many other schemes, with lower \leq O7 order versions widely used in the atmospheric sciences and \leq O9 in the gas dynamics communities. All solutions produced in this study are made with comparable or higher order numerical approximations for both interpolations wherever odd-grid calculations are needed as well as for calculations of the pressure gradient and divergence calculations in the momentum equations and divergence term in the pressure equation. Higher order (e.g. O4–18) subgrid-scale (SGS) turbulent flux approximations had little impact on solutions (Straka *et al.*, 2023 SWK23) and thus are not presented.

Odd order schemes generally have better phase errors compared to one-order lower even schemes, while even order schemes have better amplitude errors than one-order lower odd schemes (T87). None of the schemes were combined with flux limiters (e.g. Leonard, 1991 L91; BS00) for this study. Other important types of advection and flux scheme constructs, such as finite-volume, finite-element, compact, spectral/pseudo-spectral, and so forth, schemes were not considered herein, but should be considered in the future.

High order advection computations based on upwind-biased odd order and centred even order traditional flux or Crowley-type flux schemes (including higher derivative terms) can be made with constant grid-based interpolation coefficients (T87), which are based on Lagrangian interpolations and adjusted so that they have

the same order of error as pure advective schemes for constant advective velocity and grid spacing (T87; interpolation coefficients for constant grid flux are identical to the reconstruction coefficients used in WENO schemes S97). Higher order integrated flux schemes for odd and even order for traditional flux and Crowley flux schemes can also be based on unadjusted Lagrangian interpolations for either unstretched or stretched/irregular grids. While seemingly high order, their accuracy is not equivalent to pure advective schemes when the advective velocity and grid increment are constant and have been demonstrated to be less accurate (T87). Use of an analytical function and its derivative can be used to demonstrate that constant grid flux schemes converge at the order of the scheme, while integrated flux schemes only converge at O2 regardless of the order of the interpolation (SWK23, in review; thus, not shown here), consistent with T87. All non-WENO odd order schemes used in this study were one point-biased, although they could be constructed as up to N -point upwind-biased schemes, where N is order of accuracy. The reconstruction polynomials, which are used to compute the fluxes for WENO schemes, are numerically identical to the constant grid flux polynomials, but found by alternative methods (e.g. Shu, 1998). Vertical advection terms for scalars can be integrated for mode-split simulations on the slow time step, or on the fast mode time step using multiple small time steps to accommodate fast-moving gravity waves, with the former used herein.

Traditional odd and even order higher-order advection/flux schemes are simple to implement and computationally very efficient. In addition, these flux schemes are very accurate, especially for smooth flows. However, they are subject to the production of aliasing and high frequency dispersion errors, especially near sharp gradients and discontinuities (S97), and thus require the use of flux-limiters (e.g. Bott, 1989; L91; S97; BS00; Durran, 2010 etc.) and/or spatial filters (Shuman, 1957; Shapiro, 1970; S82; Purser, 1987 P87; Purser and Leslie, 1988 PL88; Durran, 2010) to control numerical “noise”, especially for low-order even-centred schemes. Odd order flux schemes, which inherently damp solutions, although to a lesser extent as accuracy is increased (e.g. TML05), typically require less spatial filtering than even order flux schemes.

Stable time integration for traditional flux schemes in compressible models with the slow modes (advection, diffusion, etc.) split from the fast modes (sound and gravity waves), called mode-split systems, can be accomplished with explicit two-stage O2 or three-stage O3 Runge–Kutta (RK) schemes (WS02), O4 RK4 schemes (Park and Lee, 2009), as well as with some filtered leapfrog schemes (Asselin, 1972; Park and Lee, 2009; Williams, 2009, 2011, 2013; Williams *et al.*, 2022), among

others (e.g. explicit O3 [for linear systems, O2 for nonlinear systems] Adams–Bashforth–Moulton: Wicker, 2009).

The forward-in-time multidimensional advective or flux form type Crowley schemes (e.g. C68) can be stabilised using properly implemented dimension-split (often called time-split) approaches or by the use of explicit cross derivatives (e.g. C68; S82; Schlesinger, 1985 S85; T87; Bott, 1989; Easter, 1993; Costa and Sempio, 1997). Crowley schemes can be used in mode-split models with the two-step approach proposed by WS02 for the velocity and pressure variables, or by solving the momentum equations on the small time step, the fast-mode part of the time integration as proposed by Walko and Avisar (2008). Most applications of Crowley schemes have used stabilising derivatives up to order N for an N -order Crowley scheme. Smolarkiewicz (1982) used a stabilising second-order derivative, but commented that the first derivative advection or flux could be approximated using any higher order scheme. As described by T87, even (odd) derivative terms in Crowley schemes mostly impact amplitude (phase) errors. Multi-dimensional, dimension-split schemes, including Crowley schemes, have been shown to produce artificial gradients (Clappier, 1998) owing to errors with diagonal advection/flux in flows with deformation for at least some systems of equations. Fortunately, these artificial gradients can be eliminated by correctly formulating the flux using a very simple flux correction, which requires minimal code changes. While WS02 suggested using the Clappier (1998) flux correction, they did not use it in their mode-split Crowley scheme demonstration using the Straka *et al.* (1993 S93) density current problem, but were still successful in using the Crowley mode-split time integration scheme. Positive definite area-preserving integrated flux Crowley schemes based on nonlinearly normalising and limiting fluxes (applicable to other types of flux schemes) for up to O4 were presented by Bott (1989) and to O5–8 by Costa and Sempio (1997), along with many others who presented variations described in the literature, and these schemes have been shown to be accurate and efficient, but are not considered herein. Finally, Smolarkiewicz (1985) showed that the time accuracy of the Crowley scheme for non-constant velocities could be increased from O1 to O2 by simply using the advecting velocity at time level $n + 1/2$, denoted by $v^{n+1/2}$, after each dimensional direction update in the advection/flux computations. Values of $v^{n+1/2}$ can be obtained by using the average of the n^* and n time level velocities $v^{n+1/2} = 0.5(v^* + v^n)$, or by using extrapolated velocities at time levels $n-1$ and n , $v^{n+1/2} = 0.5(3v^n - v^{n-1})$. However, it is not known how the WS02 mode-split Crowley affects the Smolarkiewicz (1985) procedure in attempting to achieve O2 temporal accuracy. Thus, this procedure was not used in the results presented in the current study,

as preliminary test results were somewhat encouraging to mixed.

The WENO schemes, and their many variants, are widely popular in many areas of fluid dynamics, and to a lesser extent in atmospheric and ocean sciences (e.g. Tan *et al.* 2005; TML05), and have been shown repeatedly to provide excellent solutions for non-viscous fluid problems with very complex flows and sharp boundaries/shocks. Most WENO schemes are odd order, although high order central WENO schemes for O4, 6 and 8 have been developed (e.g. Qiu and Shu, 2002), and can be more efficient than odd order WENO schemes. Care must be taken with some central WENO schemes to avoid negative linear weights. High computational cost associated with WENO schemes is perhaps one reason WENO schemes have not been used as often in atmospheric sciences compared to other schemes. Nevertheless, two O3–9 WENO scheme variations are available in Bryan's CM1 model (Cloud Model 1; Bryan, 2021 B21, <https://www2.mmm.ucar.edu/people/bryan/cm1/>), and at least one O3–9 WENO scheme variation is available in at least some versions of National Center for Atmospheric Research (NCAR)'s Weather Research and Forecast model (WRF), O3–5 WENO schemes in the Meso-NH model (Lunet *et al.*, 2017), among other models in the atmospheric and oceanic sciences (e.g. TML05 for idealised advective atmospheric related test problems). Some of the desirable characteristics of WENO schemes include being able to stably preserve gradients, maintain non-oscillatory behaviour (although WENO schemes are not necessarily monotonic) by limiting dispersion error, and minimise dissipation of extrema near steep gradients and discontinuities through the use of nonlinearly weighted combinations of upwind, downwind, and centred (for some orders) local reconstruction polynomials for the fluxes. Examples are three third order fluxes for a fifth order scheme, four fourth order fluxes for a seventh order scheme, five fifth order fluxes for a ninth order scheme, and so forth, in regions of smooth flow, yet will maintain approximately third, fourth, fifth, etc. order near discontinuities, respectively; see references above, especially S97, for comprehensive explanations and descriptions for constructing WENO schemes.

While the WENO schemes can produce excellent solutions for complex non-viscous problems, especially higher >O5 solutions, these schemes become increasingly computationally expensive, with floating-point operation (FPO) numbers related to R to the third power, where order $O = 2R - 1$. In comparison, the traditional comparably high order advection or flux schemes have FPO numbers related to order of the scheme, and Crowley schemes have FPOs numbers related to the scheme order to the second power. Much of the computational cost of WENO schemes

is associated with computing the smoothness indicators (e.g. S97; G09; Wu *et al.*, 2020 W20; Wu *et al.*, 2021 W21). However, W20 and W21 recently described simpler, very accurate smoothness indicators (exact for sine-waves), which are much more efficient than traditional $\geq O7$ WENO schemes. The WENO-Sine scheme makes the computational cost of implementing WENO related to R to the second power, rather than R to the third power for traditional WENO smoothness indicators. This cost need should not be considered excessively restrictive for using WENO schemes for numerical integration in studies of complex atmospheric problems and numerical weather prediction, as the flux computations are often only five to ten percent of the total cost (e.g. TML05). Finally, WENO schemes, as well as basic flux schemes, can be stably integrated in slow/fast mode-split models with various three-stage O3 Runge–Kutta time schemes RK3 (Williamson, 1980; Shu, 1988; Shu and Osher, 1988; WS02; Baldauf, 2008; where RK3 in general is O2 for nonlinear system time integrations and O3 for only linear system time integrations: Purser, 2007; Baldauf, 2010; Lunet *et al.*, 2017).

A hybrid-WENO-Crowley odd order dimension-split scheme is also proposed in this study in an attempt to maintain the desirable characteristics of WENO schemes and offset a portion of the computational expense of the WENO scheme when used with Runge–Kutta time integration schemes. The proposed hybrid scheme simply uses O3–17 WENO fluxes for the advection flux terms, which are then coupled with the N -derivatives required for stability for Crowley schemes, with the N -derivative differenced with higher order constant grid fluxes. Time integration is stably carried out with the WS02 mode-split forward scheme for Crowley schemes. A higher order hybrid-WENO-Crowley scheme can allow for a combination of the desirable aspects of WENO schemes when simulating flows with sharp gradients and/or discontinuities and also be amenable to stable time integration with a simpler forward scheme, which reduces computational cost relative to RK3 time integration. The hybrid-WENO-Crowley scheme can incorporate the W20 and W21 WENO-Sine smoothness indicators to further reduce computational cost.

Some motivating questions for this study include: (1) first and foremost, which of the high order numerical schemes discussed above can most accurately simulate the nonlinear diffusion-limited 2D colliding plumes test problem by providing the most accurate representation of both physically important, but marginally resolved (6–10 Δx) flow features, as well as well-resolved and smooth features of the solutions in their thermodynamic fields, kinetic energy (KE) fields, and derivative kinematic fields (e.g. deformation and vorticity), using O3–18 flux

approximations and 25–166.67 m spatial resolutions?; (2) which of these schemes can best accomplish high accuracy with high computational efficiency?; and (3) are there variations and combinations of these schemes that are more accurate and/or more efficient than the others? Objective error measures are obtained using the O17 flux scheme and 25 m grid resolution, nearly grid-converged, diffusion-limited solution of the 2D colliding plumes problem for a reference. The solutions all were integrated in time with relatively small time steps to minimize temporal truncation errors. Both a brief description of the model and a description of the design of the 2D colliding plumes problem are included in Section 2. A reference solution is then described and serves as the basis for visual comparisons and computed objective errors in Section 3, as are the results and discussion of the results. A summary of the findings and the conclusions are presented in Section 4.

2 | METHODS

The 3D fully-compressible model used in this study was based on the Euler equations cast in a conservative flux form for dry or moist dynamics on the staggered C-grid, following concepts discussed by Bryan and Fritsch (2002 BF02), Bryan and Morrison (2012), and B21, and nearly conserves mass and energy. Fast sound and gravity waves and slow advective and turbulent modes were split into a fast/slow time-split system of equations (Skamarock and Klemp, 1992), and stably integrated by including divergence damping on the fast-mode time steps (Skamarock and Klemp, 1992). The divergence damping coefficient was kept very small to minimise errors from its use (Lian *et al.*, 2023). Importantly, divergence damping differencing has formal temporal and spatial accuracy of only O1 and O2, respectively. The turbulence scheme and spatial filtering were integrated in time with accuracy of O1 forward-in-time for Crowley, and O2 for nonlinear RK3 time integrations by computing these terms on all three RK3 stages. Flux schemes used were the traditional constant grid flux, dimension-split constant grid flux Crowley (T87), and WENO flux (e.g. JS96; S97; BS00; G09). Turbulent-fluxes for all variables, except for pressure, were computed using O2 numerical approximations and a constant eddy-mixing coefficient, which allowed for a diffusion-limited nearly grid-converged reference solution when spatial (and temporal) resolution was sufficiently reduced. Extensive tests reported elsewhere (SWK23) showed that higher order (O4–18) numerical approximations for constant eddy-mixing for constant grid flux or Lagrangian integrated flux based SGS turbulent fluxes had little impact on RMS errors of fully compressible colliding plume solutions. The minimal impact

of higher order SGS turbulent fluxes was a result, at least in part, of differencing errors with diffusion terms not being propagated as much each time step as they are with advection terms, rather the diffusion term errors tend to be damped locally (e.g. personal communication, B. Fornberg, 2019). Spatial filtering was based on the family of filters described by P87. Note that the orders associated with the high order spatial filters are the orders of the derivative they are associated with and not the spatial differencing accuracy; they all are O2 accurate in space as can be seen in Fornberg's (1988) tabulations.

A descriptive summary of all numerical schemes and physics are provided in Supporting Information as Table S1 (adapted from SWK23). The Courant–Friedrichs–Lewy (CFL) conditions and critical wave number for stable RK3 solutions with linear odd and even order O1–20 advection/flux approximations following procedures described by Baldauf (2008), and for stable leapfrog even order O2–20 advection/flux approximations following Haltiner and Williams (1980), Fornberg (1987), and Straka and Anderson (1993) for comparison, are tabulated in Appendix A as Tables A1, A2 and A3, respectively. All constant grid flux differencing, interpolation coefficients, staggered grid coefficients for pressure gradient and divergence calculations for O1–20 schemes, and filter coefficient for even orders O2–20 are tabulated in Supporting Information Tables (S2a–d) along with instructions for reproducing the reported values. The reader is referred to JS96, S97, BS00, S03, Borges *et al.* (2008) and G09 for instructions to construct WENO schemes as well as all coefficients. Note that the nonlinear weights for WENO schemes were found using improved methods from Borges *et al.* (2008), rather than those proposed by Jiang and Shu (1996). Additionally, the nonlinear weights for O3, 7, 11 and 15 WENO schemes suggested by Castro *et al.* (2011) are used. Finally, a value of $\epsilon_{\min} = 1 \times 10^{-10}$ (BS00) is used to prevent division by zero in computation of the nonlinear weights for the WENO scheme, while a value of $\epsilon_{\max} = 1 \times 10^{30}$ is used to keep the numerator in the weights from exceeding machine precision (64 bits). The exponent parameter p in the nonlinear weights for WENO fluxes can have an impact on the nonlinear dissipation, but not the formal accuracy of the WENO fluxes (e.g. JS96; S97; G09). This nonlinear dissipation can increase with an increasing p (e.g. G09), and thus, increasing the p can result in better control of overshoots at very sharp boundaries and shocks. Traditionally, the value of the exponent of $p = 2$ is used (e.g. JS96; S97; BS00; etc.); however, a value of $p = r$ has been shown by G09 to result in more accurate solutions. The majority of WENO flux solutions shown and discussed herein are made with $p = 2$, with test solutions produced and discussed for $p = r$.

Results from a comprehensive suite of simulations of a dry nonlinear 2D test problem are presented

to demonstrate the impact of very-high order finite difference flux, dimension-split Crowley flux, and WENO flux schemes made using odd/even order O3/4, O5/6, O9/10, O13/14 and O17/18 numerical approximations (odd order only for WENO), combined with comparable even order Lagrangian interpolations for information required at off-grid point locations and even order staggered pressure gradient/divergence approximations (one order higher for odd order schemes; e.g. for O17 advection, O18 interpolation/pressure gradient/divergence is used). Since most studies in atmospheric sciences use at most O2–7 advection/flux, the lowest order of numerical approximations shown are O3/4. Flux correction for diagonal advection (Clappier, 1998) is not used for the Crowley solutions, nor was this relatively simple correction necessary, as was also found by WS02. Simulation results for O1/2, O7/8, O11/12 and O15/16 are not shown for brevity. A summary of the spatial resolutions (166.66 ... (hereafter 166.67), 133.33 ... (133.33), 100, 66.66 ... (66.67), 50, 33.33 ... (33.33), and 25 m, time steps and domain parameters used herein, is presented in Table 1. The orders of accuracy for fluxes, interpolations, and pressure gradient/divergence that comprise the simulation Sets A–H are presented in Table 2. All solutions were made with 64-bit mathematics, noting that round-off errors limit solution improvement beyond ~O17/18 or O19/20 for all schemes considered. Solutions in this article were produced with the Intel compilers; 128-bit arithmetic and storage was not available with the latest Intel and GNU FORTRAN compilers.

2.1 | Efficient implementation of the Crowley schemes

The computational efficiency of an N -order Crowley scheme with N derivatives can be substantially improved, especially when a model has many scalar dependent variables. Consider the O4 flux Crowley scheme, for example, with fluxes for grid index i for some variable $b(i)$, given by:

$$\text{Flux}(i+1/2) = s1 + s2 + s3 + s4,$$

where

$$s1 = (a^1) \bullet (c11 \bullet b(i-1) + c12 \bullet b(i) + c13 \bullet b(i+1) + c14 \bullet b(i+2)),$$

$$s2 = (a^2) \bullet (c21 \bullet b(i-1) + c22 \bullet b(i) + c23 \bullet b(i+1) + c24 \bullet b(i+2)),$$

$$s3 = (a^3) \bullet (c31 \bullet b(i-1) + c32 \bullet b(i) + c33 \bullet b(i+1) + c34 \bullet b(i+2)),$$

$$s4 = (a^4) \bullet (c41 \bullet b(i-1) + c42 \bullet b(i) + c43 \bullet b(i+1) + c44 \bullet b(i+2)).$$

TABLE 1 Domain and time-step parameters.

Δx (m)	Δz (m)	L_x (m)	L_z (m)	N_x	N_z	$N_x \bullet N_z$	N_t	Δt (s)
166.66 ...	166.66 ...	20,000	10,000	121	61	7,381	1,920	0.520833 ...
133.33 ...	133.33 ...	20,000	10,000	151	76	11,476	2,400	0.4166 ...
100.00	100.00	20,000	10,000	201	101	20,301	3,200	0.3125
66.66 ...	66.66 ...	20,000	10,000	301	151	45,451	4,800	0.20833 ...
50.00	50.00	20,000	10,000	401	201	80,601	6,400	0.15625
33.33 ...	33.33 ...	20,000	10,000	601	301	180,901	9,600	0.104166 ...
25	25	20,000	10,000	801	401	321,201	12,800	0.078125

Note: N_x (N_z) is equal to the number of scalar grid points in x - (z -) directions for a staggered grid. The total number of grid points = $N_x \bullet N_z$, and N_t is the number of time steps for 1,000 s of integration. The x -direction velocity (u) has one extra point in the x -direction and the z -direction velocity (w) has one extra point in the z -direction for the staggered C -grid. The time steps for each resolution are found using $\Delta t = C \bullet \Delta x / V_{\max}(s)$, where Courant number $C = 0.046875$, values of Δx are grid resolutions, and approximate maximum velocity $V_{\max} = 15 \text{ m}\cdot\text{s}^{-1}$.

$a = u \Delta t / \Delta x$, is the Courant number with velocity, time step, and grid spacing given by u , Δt , Δx , respectively, c_{ji} and below $c(j, i + [-1, 0, 1, 2])$ are stencil coefficients to compute fluxes, and $s1-4$ are the terms for the O1-4 fluxes, respectively. (Note the dot \bullet denotes multiplication.)

The fluxes can be rewritten for better computational efficiency as:

$$\text{Flux}(i+1/2) = t1 \bullet b(i-1) + t2 \bullet b(i) + t3 \bullet b(i+1) + t4 \bullet b(i+2),$$

where

$$\begin{aligned} t1 &= a \bullet (c11 + a \bullet (c12 + a \bullet (c13 + a \bullet (c14)))) , \\ t2 &= a \bullet (c21 + a \bullet (c22 + a \bullet (c23 + a \bullet (c24)))) , \\ t3 &= a \bullet (c31 + a \bullet (c32 + a \bullet (c33 + a \bullet (c34)))) , \\ t4 &= a \bullet (c41 + a \bullet (c42 + a \bullet (c43 + a \bullet (c44)))) . \end{aligned}$$

The Crowley flux term here can be written with more compact notation as:

$$\text{Flux}(i+1/2) = t(1) \bullet b(i-1) + t(2) \bullet b(i) + t(3) \bullet b(i+1) + t(4) \bullet b(i+2),$$

where

$$t(j) = a \bullet (c(j, i-1) + a \bullet (c(j, i) + a \bullet (c(j, i+1) + a \bullet (c(j, i+2)))) \text{ for } j=1, 4.$$

Importantly, the values for $t1$, $t2$, $t3$ and $t4$, or $t(j)$ in the improved efficiency version, only need to be computed once (twice) per time step for scalars (velocity and pressure) and can be reused for each scalar in the time step. Also, the variable “ a ” does not have to be repeatedly taken to an integer power. Furthermore, the improved efficiency version requires dependent variables at each index in the difference stencil for scalars to be accessed only once (for the O4 flux example a total of four dependent variable accesses versus 16), both of which can be very advantageous, in terms of computer CPU and cache use, especially in models with a large number of scalar dependent

variables, which is often the case for models that include aerosols, microphysics and chemistry. This procedure theoretically results in the computational cost for even (odd) order Crowley flux schemes being equal to (twice) the “traditional” odd order flux computational cost each time the flux needs to be computed. In other words, the FPO numbers become linearly related to the scheme order rather than the scheme order squared.

2.2 | Two-dimensional colliding plumes test problem

To compare the performance of a comprehensive suite of simulations using five numerical schemes, each with five orders of accuracy, and eight grid resolutions, a 2D nonlinear test problem with warm and cold spheroidal plumes colliding with each other above the ground was used. This problem was similar to the one described in Norman (2021 N21), although with eight times smaller initial plume perturbation amplitude, as well as with inclusion of constant eddy-mixing SGS turbulent fluxes. The constant eddy-mixing SGS turbulent fluxes allow for a nearly grid-converged solution for nonlinear problems if the spatial resolution is fine enough. In addition, the effects on solutions of a background mean wind of $U_t = -20 \text{ m}\cdot\text{s}^{-1}$ were also considered. As the plumes approach each other, vertical gradients are enhanced, and after colliding, both cold and warm air plumes spread out laterally while thermal and shear instabilities result in the development of prominent rotors. The solutions are symmetric in the horizontal, but they are not symmetric in the vertical owing to vertical gradients in density, temperature, pressure, and sound speed. Rotors of different sizes develop as the plumes spread laterally, with the rotors tending to grow upscale owing to the 2D slab-symmetry geometry of

TABLE 2 Simulation sets, resolutions, and orders of accuracy.

Set	Schemes	Experiment description	$\Delta x = \Delta z$ (m)	Order flux	Order of SF/PD/I
A	Co, Ce, Fo, Fe, W	Co, Ce, Fo, Fe, W With $U_i = 0 \text{ m}\cdot\text{s}^{-1}$	25, 33.33, 50, 66.67, 100, 133.33, 166.67	O3, 5, 9, 13, 17 O4, 6, 10, 14, 18	O18/Oc/Oc
B	Co, Ce, Fo, Fe, W	Co, Fo, Fe, W With $U_i = -20 \text{ m}\cdot\text{s}^{-1}$	25, 33.33, 50, 66.67, 100, 133.33, 166.67	O3, 5, 9, 13, 17 O4, 6, 10, 14, 18	O18/Oc/Oc
C	WS WR	WS (W-sine, $p = 1$) WR ($p = R$)	100	O3, 5, 9, 13, 17	O18/Oc/Oc
D	WL c:c:17	WL (WH) has low (high) order WENO for first two stages of RK3 time integrations	100	O3, 5, 9, 13, 17	O18/O18/O18
WH17:17:c					
WH Plc					
E	Ws Fv Wv fs	Ws Fv is W for scl, Fo for vp Wv fs is W for vp, Fo for scl	100	O3, 5, 9, 13, 17	O18/O18/O18
F	C2	Co with $N = 2$ derivatives	100	O3, 5, 9, 13, 17	O18/Oc/Oc
G	Hy, HS Hs cv Hv Cs	Hy W/Co, Hy W-sine ($p = 1$)/Co Hy scl and Co vp Hy vp and Co scl	100	O3, 5, 9, 13, 17	O18/Oc/Oc
H	Fv s17 Fs v17	Fo vp, O17 scl Fo sc, O17 vp	100	O3, 5, 9, 13, 17	O18/O18/O18

Abbreviations: Co = odd order upwind-biased constant grid flux Crowley; Ce = even order constant grid flux Crowley; Fo = upwind-biased odd order constant grid flux; Fe = even order constant grid flux; W = WENO flux; WS = W with sine-based smoothness indicators; WR = W with smoothness indicator power given by $p = R$, where $O = 2R - 1$; WL c:c:17 = O3, 5, 9, 13, 17 W for stages one and two of RK3, and O17 W for stage three of RK3; WH = (17:17:c) = O17 W for stages one and two of RK3, and O3, 5, 9, 13, 17 W for stage three of RK3 with comparable order interpolations and pressure gradient/divergence; Ws Fv = W for scalars and Fo for velocities/pressure; Wv fs = W for scalars and Fo for velocities/pressure; C2 = O3, 5, 9, 13, 17 Co with $N = 2$ derivatives in place of N = Nth order Crowley scheme; Hy = hybrid WENO/Crowley flux with sine-based smoothness indicators ($p = 1$); Hs Cv = hybrid W for scalars and Co for velocities/pressure; Hv Cs = hybrid W for velocities/pressure and Co for scalars; Fv s17 = lower order Fo (O3, 5, 9, 13, 17) for velocities/pressure and O17 Fo for scalars; and Fs v17 = lower order Fo (O3, 5, 9, 13, 17) for scalars and O17 for velocities/pressure. Other abbreviations are U_i = added mean wind; scl = scalar, vp = velocity/pressure; SF = spatial filter; PD = pressure gradient and divergence; and I = interpolations; Oc = comparable order (same order as even order flux and one order higher for odd order flux).

the domain (e.g. Fjortoft, 1953; Soong and Ogura, 1973); Appendix B includes a figure, zoomed on the left member of the symmetric circulation couplet of the colliding plumes after 1,000 s using O17 fluxes, and 16.66 ... m resolution, in which the features discussed with respect to the results herein are denoted (the upper and lower rotors, etc.) to facilitate solution of comparisons of the schemes with various orders of accuracy and resolution. The 2D colliding plume simulations produce steep gradients with strong deformation, rotation, divergence and translation kinematic characteristics, which can significantly challenge numerical schemes. The colliding plume problem has physical features and attributes, such as very sharp gradients, deformation and rotational characteristics, and smoother flow regions, which spatial grids can resolve to varying degrees. All simulations were made without the complications of physical parametrizations other than the turbulence scheme with a constant eddy diffusion coefficient and selective higher order spatial filters.

The atmosphere represented in the simulations is initially dry adiabatic (potential temperature equal to 300 K at all heights). The two plumes which collide are initiated horizontally in the centre ($x = 10$ km) of a 20×10 km x - z domain, which is periodic in the x -direction. The warm plume is centred at height $z = 3,050$ m and the cold plume is centred at height $z = 7,050$ m. The warm and cold plumes are prescribed by the same cosine squared function, but with potential temperature excess/deficit of $\Delta\theta = \pm 2.5$ K, respectively. The radii of both plumes are 2,000 (2,000) m in the x - (z -) directions. All schemes were tested with grid resolutions of $\Delta x = \Delta z = 25, 33.33, 50, 66.67, 100, 133.33, 166.67$ m. The time steps assume a constant Courant number ($C = 0.046875$) with the resulting time steps given as $\Delta t = 0.078125, 0.1041166 \dots, 0.15625, 0.20833 \dots, 0.3125, 0.4166, \text{ and } 0.520833 \dots$ (Table 1). With these values all solutions are stable, although all solutions were stable with Courant numbers as large as $C = 0.12$, and much larger if the number of small time steps was increased. The small Courant number helped keep temporal truncation errors minimised, as discussed in SWK23. A constant eddy mixing coefficient ($K_m = 10.0 \text{ m}^2 \cdot \text{s}^{-1}$) was applied to all variables (except pressure), which allowed for a nearly grid-converged solution when $\Delta x = \Delta z = 25$ m. A weak scale-selective O18 spatial filter (S82; P87; PL88; Knierel et al. 2007) was applied in both x - and z -directions to perturbation values (from their base state; pressure was not filtered). The very small filtering coefficient used ($\alpha = 0.03$) meant 2Δ spatial waves were damped 3% every time step. For comparison, a value of $\alpha = 0.24$ is used in the Weather Research Forecast model (WRF; K07). The numerical spatial filter (P87) is very selective for higher wave number (small Δx) with coefficients for the O18 filter based on the two parameters R (rolloff) and S (smoothness); (R ,

S) = (18, 0) for all solutions in this article. The spatial filter was not technically required to be as strong with odd order, upwind-biased flux scheme solutions as that needed for even order scheme solutions, and was not required at all for WENO scheme solutions; therefore, an intermediate filter coefficient α (held constant for all the schemes) was chosen so as to not overly smooth the odd order scheme solutions, or to not excessively under-smooth the even order scheme solutions. Much lower values of α were able to be used for odd order schemes where higher values of α were found to be generally detrimental. On the other hand, the lower order even scheme solutions used in this article would have significantly benefited from much stronger spatial filtering to remove large amplitude, high frequency numerical noise (dispersion error and aliasing) in the solutions presented. Use of stronger filtering for either odd or even higher order solutions would have resulted in unneeded and detrimental excessive damping of the higher order solutions. Use of a spatial filter with an order less than the order of advection/flux advection was always detrimental to the accuracy of solutions (P87, PL88), but the converse was not true.

3 | RESULTS AND DISCUSSION

3.1 | Reference solution

A nearly grid-converged reference solution (Figure 1) was produced in order to make visual solution comparisons and calculate objective error measures based on a solution made using the odd order O17 upwind-biased constant grid flux, O18 spatial filter, O18 pressure gradient /divergence, constant eddy mixing coefficient $K_m = 10.0 \text{ m}^2 \cdot \text{s}^{-1}$, $\Delta x = \Delta z = 25$ m, and $\Delta t = 0.078125$ s in order to make visual solution comparisons and calculate objective error measures. The idea of nearly grid-converged solutions herein means the flow and scalar fields become sufficiently resolved and smooth for the resolution such that the higher order derivatives become increasingly well posed and well behaved as a result of the constant eddy-mixing turbulent diffusion (or in other studies by flux-limiters; e.g. N21). As Park and Lee (2009) note, in the context of time differencing for nonlinear problems, "... the theory that a smaller time step with a low-order time-integration scheme can be better than an inefficient high-order scheme is supported only when the convergence rule is maintained" (i.e. for a linear problem). The same holds in the context of spatial differencing in that a higher spatial resolution with low-order spatial differencing can be better than a computationally intensive high order scheme. As a consequence of these concepts, "convergence" of nonlinear solutions in this study only

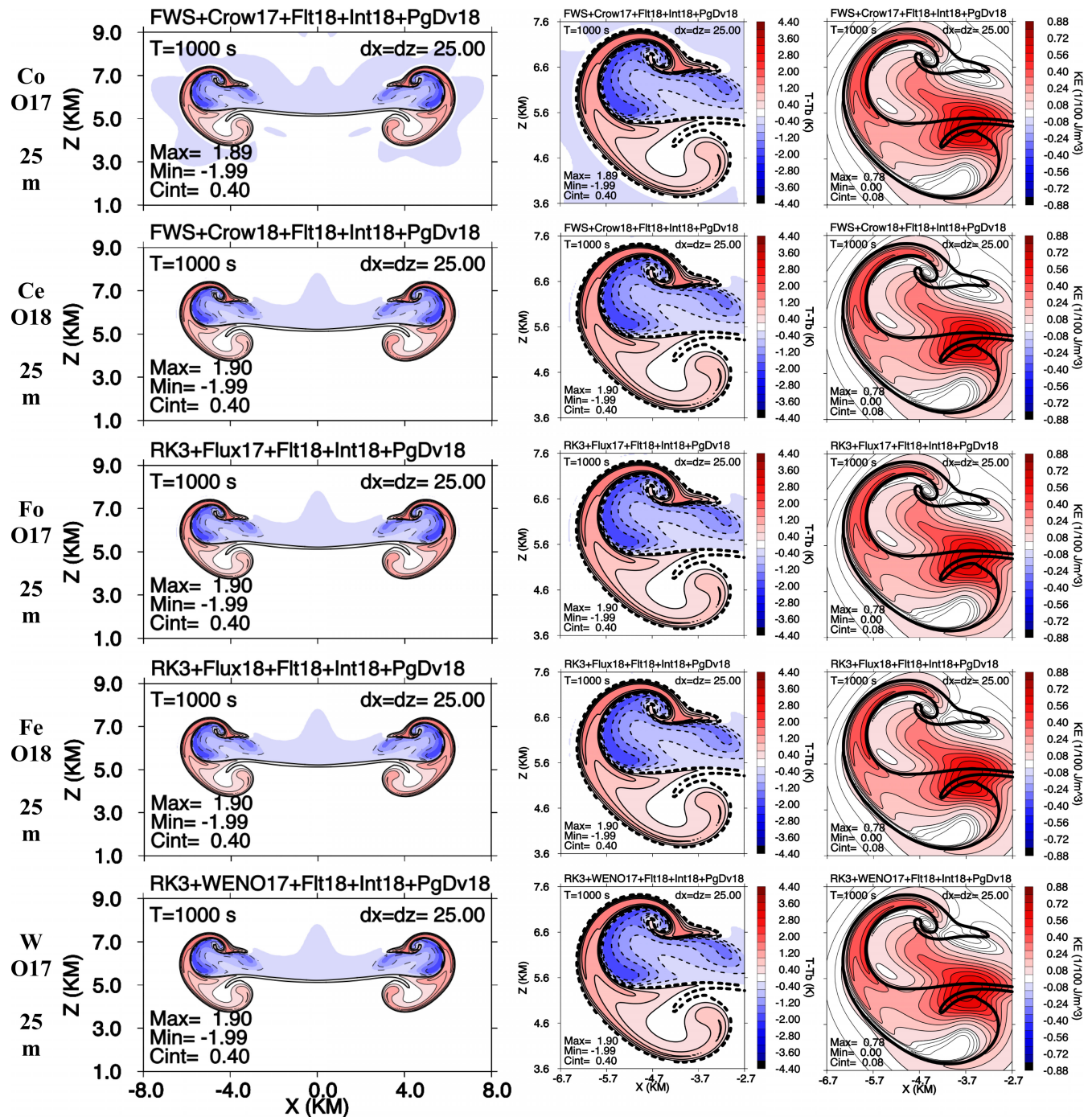


FIGURE 1 Set A perturbation potential temperature ($T - T_b$; K) fields at $t = 1,000$ s made with grid resolution $\Delta x = \Delta z = 25$ m with odd/even order O17/18 upwind-biased/centred constant grid flux Crowley (Co = odd; Ce = even), upwind-biased/centred constant grid flux (Fo = odd; Fe = even), and odd order WENO (W) flux schemes, all with O18 interpolations and pressure gradient/divergence, O18 spatial filter, same Courant number C , and constant eddy mixing coefficient of $K_m = 10 \text{ m}^2 \text{ s}^{-1}$ shown in left and centre columns. Kinetic Energy per unit volume (KE; $1/100 \text{ J} \cdot \text{m}^{-3}$) fields shown in the right column. Maximum (Max) and minimum (Min) values and contour interval (Cint) values are on each plot. The bold solid line is the 0.2 K perturbation potential temperature contour of the simulation in the plot. The bold dashed line in the centre column plots is the 0.2 K perturbation potential temperature contour of the upwind-biased constant grid flux O17, 25 m reference solution. Only a sub-domain (most of the whole domain) from $x = -8$ to 8 km and $z = 1$ to 9 km in the left column, $x = -6.7$ to -2.7 km and $z = 3.6$ to 7.6 km (left rotor) in the centre column and right column are shown. [Colour figure can be viewed at wileyonlinelibrary.com]

means that the objective error measures are improving rather than converging at the theoretical linear convergence rates.

Objective error measures such as root-mean-square (RMS) errors and L_∞ error norms (Figure 2), computed

for all schemes using the 25 m reference solution, for resolutions of $\Delta x = \Delta z = 25, 33.33, 50, 66.67, 100, 133.33$ and 166.67 m and fluxes of O3/4, 5/6, 9/10, 13/14 and 17/18 were used to determine which resolution could be best used for a reference solution. In addition, Richardson

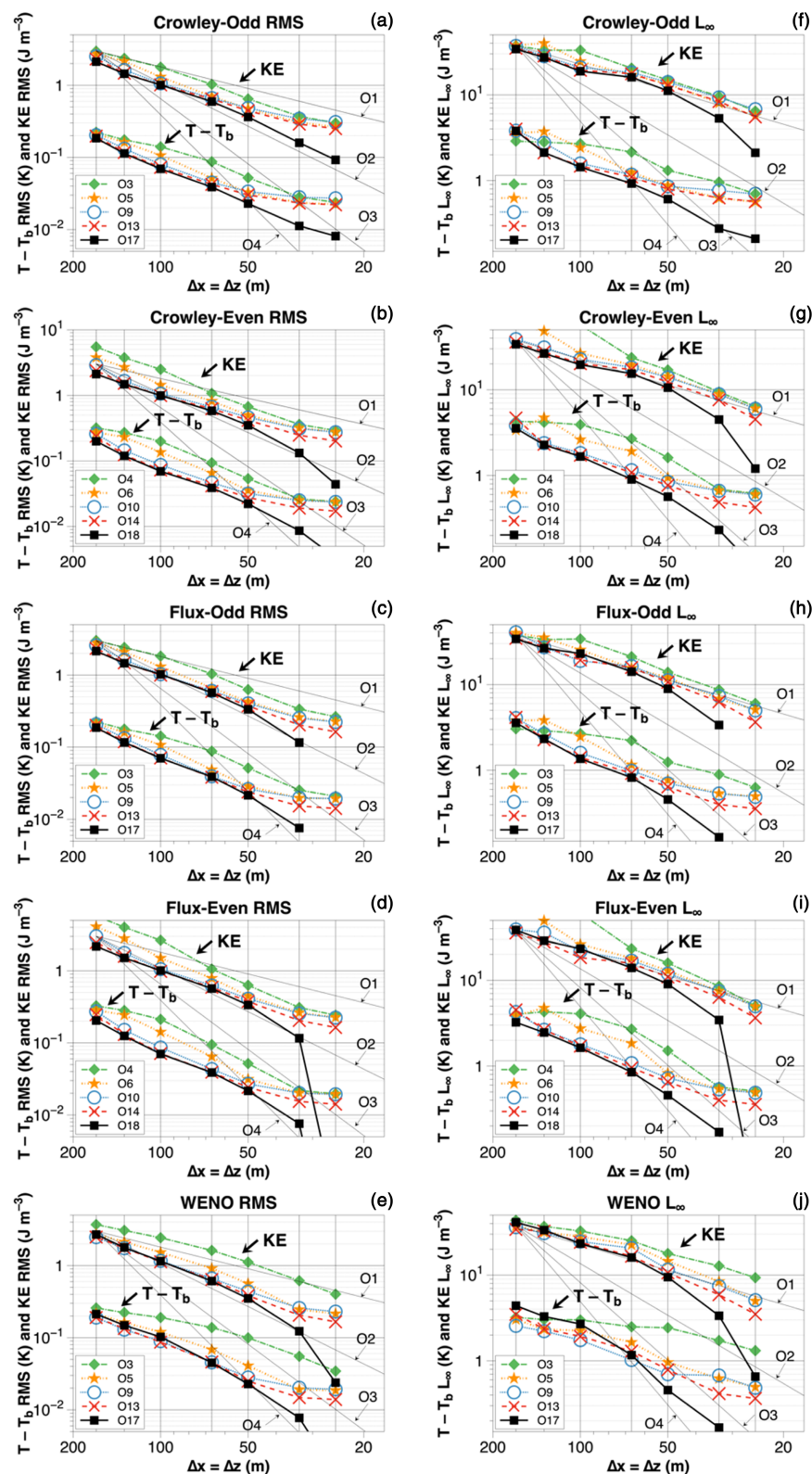


FIGURE 2 Set A objective error measures versus resolution $\Delta x = \Delta z$ (m) for orders of accuracy (legend). Perturbation potential temperature ($T - T_b$; K; lower curve cluster in each panel) and Kinetic Energy (KE; $J m^{-3}$; upper curve cluster in each panel) Root Mean Square errors (RMS; left) and L_∞ error norms (right) calculated against the upwind-biased constant grid flux O17, 25 m reference solution for the odd/even O3/4, 5/6, 9/10, 13/14 and 17/18 order upwind-biased/centred constant grid flux Crowley schemes, odd/even order upwind-biased/centred constant grid flux, and odd order O3, 5, 9, 13 and 17 WENO flux schemes, all with comparable order interpolations and pressure gradient/divergence, O18 spatial filter, same Courant number C , and constant eddy mixing coefficient of $K_m = 10 m^2 s^{-1}$. [Colour figure can be viewed at wileyonlinelibrary.com]

extrapolation (not shown) based on the $\Delta x = \Delta z = 25$ and 33.33 m solutions was used, as in S93, to support that the test problem solution was sufficiently grid-converged with O17 numerical approximations and $\Delta x = \Delta z = 25$ m resolution. Note that, phase errors (which vary with each scheme, as some of the solutions were not completely grid-converged for the nonlinear test problem) produced localised differences amongst the schemes. For example, in some test solutions, there were local differences from the reference solution of up to ~ 0.21 K in the perturbation potential temperatures, even though the simulation extrema (L_{\max} and L_{\min} error norms calculated against the reference solution) were identical to about four digits for all variables. Finally, as described in SWK23 for this colliding plumes problem, the L_1 error norms for perturbation potential temperature between O3–17, 33.33 m simulations and O17, 25 m simulation, were $\sim 4.12 \times 10^{-3}$ to 1.16×10^{-3} , while L_1 error norms between the O3–17, 50 m and O17, 25 m solutions, ranged from $\sim 4.81 \times 10^{-3}$ to 3.79×10^{-3} . These error norms met the Zhang *et al.* (2003) L_1 error norm < 0.01 criteria to indicate near-convergence for their viscous Rayleigh–Taylor problem. The L_1 error norms 3.71×10^{-2} to 2.64×10^{-2} between O3–17, 100 m solutions and O17, 50 m solutions indicated that the 100 m solutions were not near-convergence based on the Zhang *et al.* (2003) criteria.

Using a spatial resolution of $\Delta x = \Delta z = 25$ m with any of the schemes produced maxima and minima in the perturbation potential temperature, winds, and perturbation pressure fields that were generally within 0.51% of each other, with the O17, 25 m Crowley solution having the largest of these differences and largest RMS errors, and the O18 flux, O17 WENO, and O18 Crowley having the smallest differences and RMS errors from best to worst, respectively. Regardless, any of these $\Delta x = \Delta z = 25$ m solutions made with O17/18 numerical approximations from any of the schemes in Set A were nearly indistinguishable and had very nearly identical maxima and minima for up to three to four digits, as well as comparable RMS errors and L_∞ error norms. As a result, any of the O17/18, 25 m solutions made could have been used as a reference solution, without any change in the conclusions based on objective error measures (and visual appearances; analyses with different reference solutions are not shown for brevity). The O9/10–17/18 solutions made with $\Delta x = \Delta z = 25$ also were visually, very nearly indistinguishable from the reference simulation solution without any added mean wind, as were the O13/14–17/18, 25 m solutions made with an added mean wind of $U_t = -20 \text{ m s}^{-1}$. Finally, it should be kept in mind that numerical errors of any sort can result in buoyancy and shear instabilities to be erroneously excited or damped in problems such as the colliding plumes problem, single

plume problems (Grabowski and Clark, 1991), and so forth, and can complicate discernment of differences owing to physical causes from those caused by numerical solution errors (Zhang *et al.*, 2003).

3.2 | Comparisons without an added mean wind (Set A)

The results from all of the schemes without an added mean wind were compared at $t = 1,000$ s by examining solutions from all schemes made with comparably high order interpolation and pressure gradient/divergence approximations, same O18 spatial filter, same Courant number C , and $\Delta x = \Delta z = 100$ m for perturbation potential temperature (Figure 3; Set A). Additional comparisons at $t = 1,000$ s are shown for solutions with enhanced focus on the vicinity of the marginally resolved upper rotor (Figures 4–8) where the largest errors generally occurred for the odd order Crowley (Co; note even order Crowley Ce not shown in Figures 4–8, but included in Supporting Information S3), odd and even constant grid flux (Fo and Fe, respectively), and WENO (W) flux schemes, comparable order interpolations and pressure gradient/divergence, same O18 filter, same Courant number C , and resolutions of $\Delta x = \Delta z = 33.33$, 66.67 and 100 m for perturbation potential temperature (Figure 4), difference plots of potential temperature between the upwind-biased constant grid flux O17, 25 m reference solution and test solutions (Figure 5), kinetic energy per unit volume [Figure 6; $\text{KE} = 0.5 \rho (u_i \bullet u_i)$], 2D vorticity in the x - z plane [Figure 7; $(\Delta u / \Delta z - \Delta w / \Delta x)$ hereafter vorticity], and total magnitude of 2D deformation in the x - z plane [Figure 8; $[(\Delta w / \Delta x + \Delta u / \Delta z)^2 + (\Delta u / \Delta x - \Delta w / \Delta z)^2]^{1/2}$; hereafter deformation], where u_i are the $i = 1, 2, 3$ (u, v, w) velocity components in m s^{-1} , and ρ is the dry air density in kg m^{-3} .

As expected, higher order numerical approximations produce visually better results with respect to the upwind-biased constant grid flux O17, 25 m reference solution for all schemes for $\Delta x = \Delta z = 33.33$, 66.67 and 100 m resolutions, especially in terms of preserving the shape of the rotors. All odd/even flux and odd/even order Crowley schemes, especially the $\geq \text{O9/10}$ higher order odd and even schemes, and $\leq \text{O6}$ even schemes, using resolutions of 66.67 and 100 m (as well as 50, 133.33 and 166.67 m not shown) produced notable ($\sim \geq 1\%$; locally as high 20%–40%) overshoots in the maxima and minima of perturbations compared to the reference solution, while these overshoots were only found in the $\leq \text{O5}$, 25 and 33.33 m solutions (former not shown). In contrast, the $\leq \text{O9}$, 100 m, and $\leq \text{O13}$, 50 (not shown) and 66.67 m, the $\geq \text{O17}$, 25 (Figure 1) and 33.33 m (Supporting Information Figure S4a) WENO flux solutions did not produce

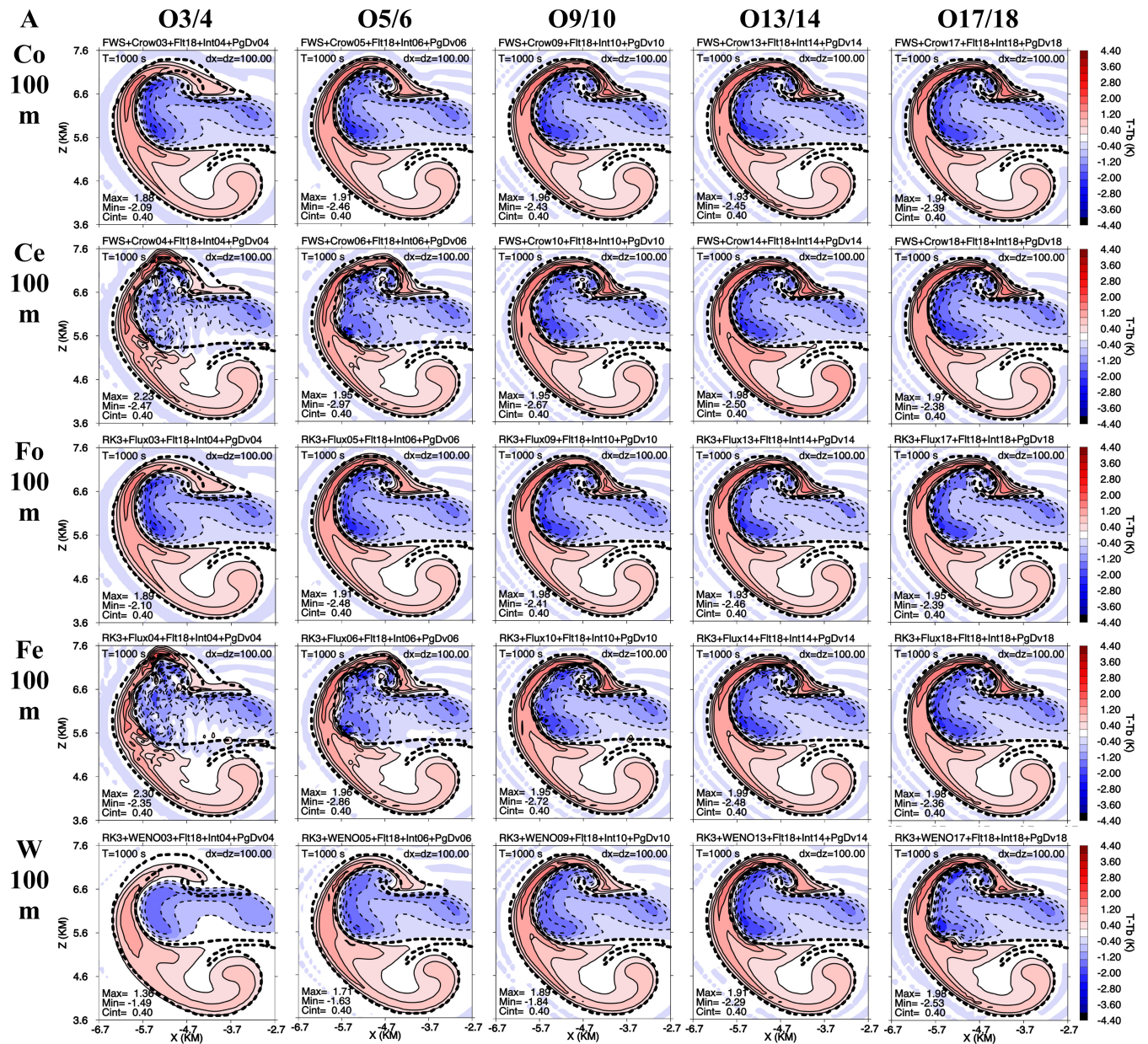


FIGURE 3 Set A perturbation potential temperature ($T - T_b$; K) fields at $t = 1,000$ s made with grid resolution $\Delta x = \Delta z = 100$ m, with odd/even order O3/4, 5/6, 9/10, 13/14 and 17/18 upwind-biased/centred constant grid flux Crowley (Co = odd; Ce = even), odd/even order upwind-biased/centred constant grid flux (Fo = odd; Fe = even), and odd order WENO flux (W) schemes, comparable order interpolations and pressure gradient/divergence, O18 spatial filter, same Courant number C , and constant eddy mixing coefficient of $K_m = 10 \text{ m}^2 \text{ s}^{-1}$. Maximum (Max) and minimum (Min) values and contour interval (Cint) values are on each plot. The bold dashed line is the 0.2 K perturbation potential temperature contour of the upwind-biased constant grid flux O17, 25 m reference solution interpolated to the grid in the plot. Only a left-side sub-domain from $x = -6.7$ to -2.7 km and $z = 3.6$ to 7.6 km is shown. [Colour figure can be viewed at wileyonlinelibrary.com]

notable ($\sim 1\%$) overshoots in the maxima and minima of perturbations compared to the reference solution. These behaviours are generally in agreement with G09 where $\leq O9$ WENO fluxes had few or no overshoots in the maxima and minima of the scalar quantity (nearly monotonic), while $\geq O13$ WENO fluxes did (not monotonic).

In spite of the overshoots, which tended to be very localized, the higher order solutions had better overall

amplitude and phase errors, as well as better objective error measures including RMS errors and L_∞ error norms for potential temperature and KE made using the constant grid flux O17, 25 m reference solution (Figure 2; RMS and L_∞). The RMS errors for potential temperature and KE fields for all schemes made with $\Delta x = \Delta z = 100$ m are also shown in Table 3. By $t = 1,000$ s, most schemes for the nonlinear problem used in this article converged

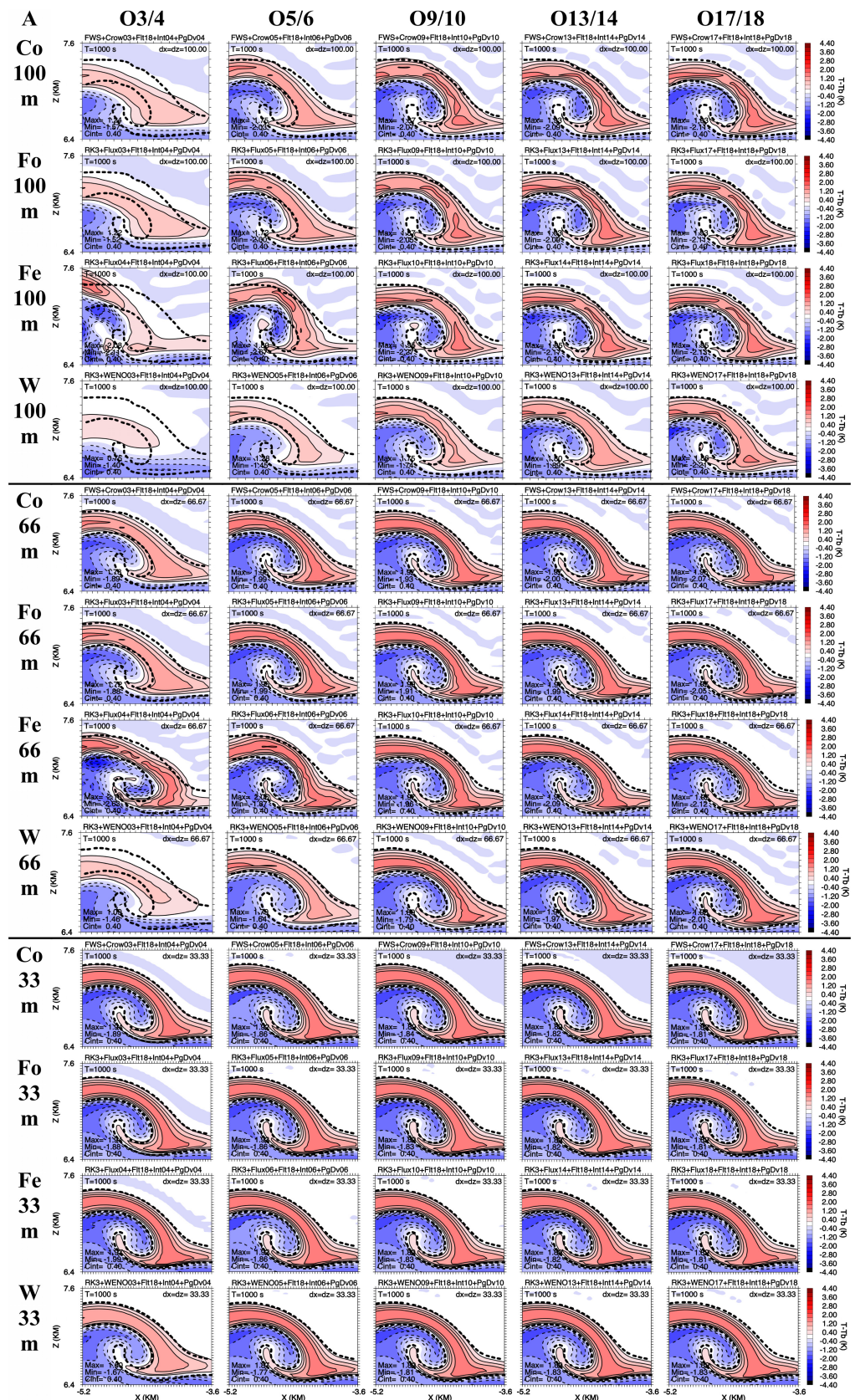


FIGURE 4 Set A perturbation potential temperature ($T - T_b$; K) fields at $t = 1,000$ s made with grid resolutions $\Delta x = \Delta z = 100, 66.67$ and 33.33 m, with odd order O3, 5, 9, 13 and 17 upwind-biased constant grid flux Crowley (Co), odd/even order O3/4, 5/6, 9/10, 13/14 and 17/18 upwind-biased/centred constant grid flux (Fo = odd; Fe = even), and odd order O3, 5, 9, 13 and 17 WENO flux (W) schemes, comparable order interpolations and pressure gradient/divergence, O18 spatial filter, same Courant number C , and constant eddy mixing coefficient of $K_m = 10 \text{ m}^2 \text{ s}^{-1}$. Maximum (Max) and minimum (Min) values and contour interval (Cint) values are on each plot. The bold dashed line is the 0.2 K perturbation potential temperature contour of the upwind-biased constant grid flux O17, 25 m reference solution interpolated to the grid in each plot. Only a zoomed-in sub-domain from $x = -5.2$ to -3.6 km and $z = 6.4$ to 7.6 km on the left side of the simulation domain is shown. [Colour figure can be viewed at wileyonlinelibrary.com]

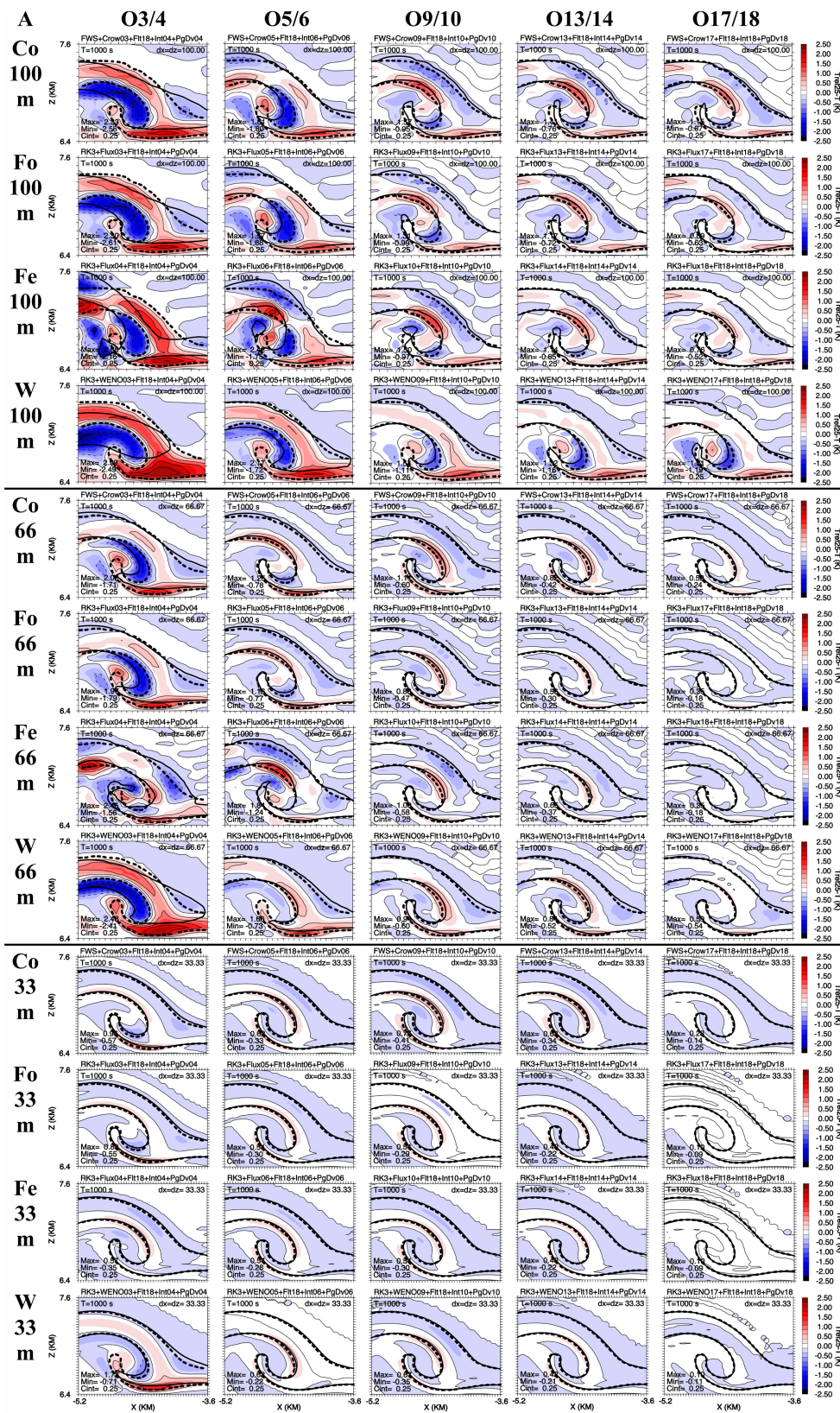


FIGURE 5 As in Figure 4, except for the difference between reference and test potential temperature ($T_{\text{Ref}} - T$; K). The bold dashed line is the 0.2 K perturbation potential temperature contour of the upwind-biased constant grid flux O17, 25 m reference solution interpolated to the grid in each plot. The bold solid line is the 0.2 K perturbation potential temperature contour of the simulation in the plot. [Colour figure can be viewed at wileyonlinelibrary.com]

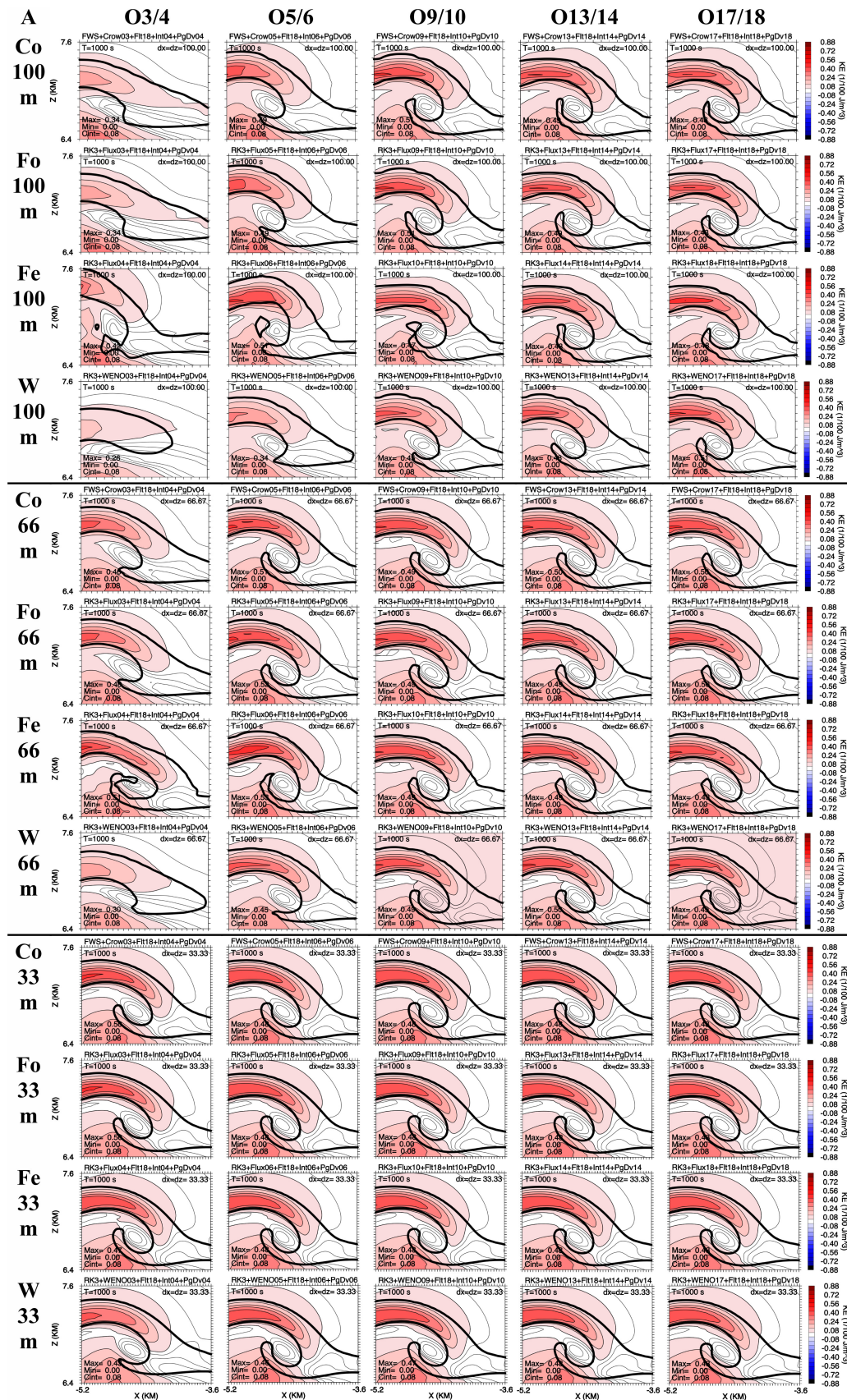


FIGURE 6 As in Figure 5, except for Kinetic Energy per unit volume (KE; 1/100 J·m⁻³). The bold solid line is the 0.2 K perturbation potential temperature contour of the simulation in the plot. [Colour figure can be viewed at wileyonlinelibrary.com]

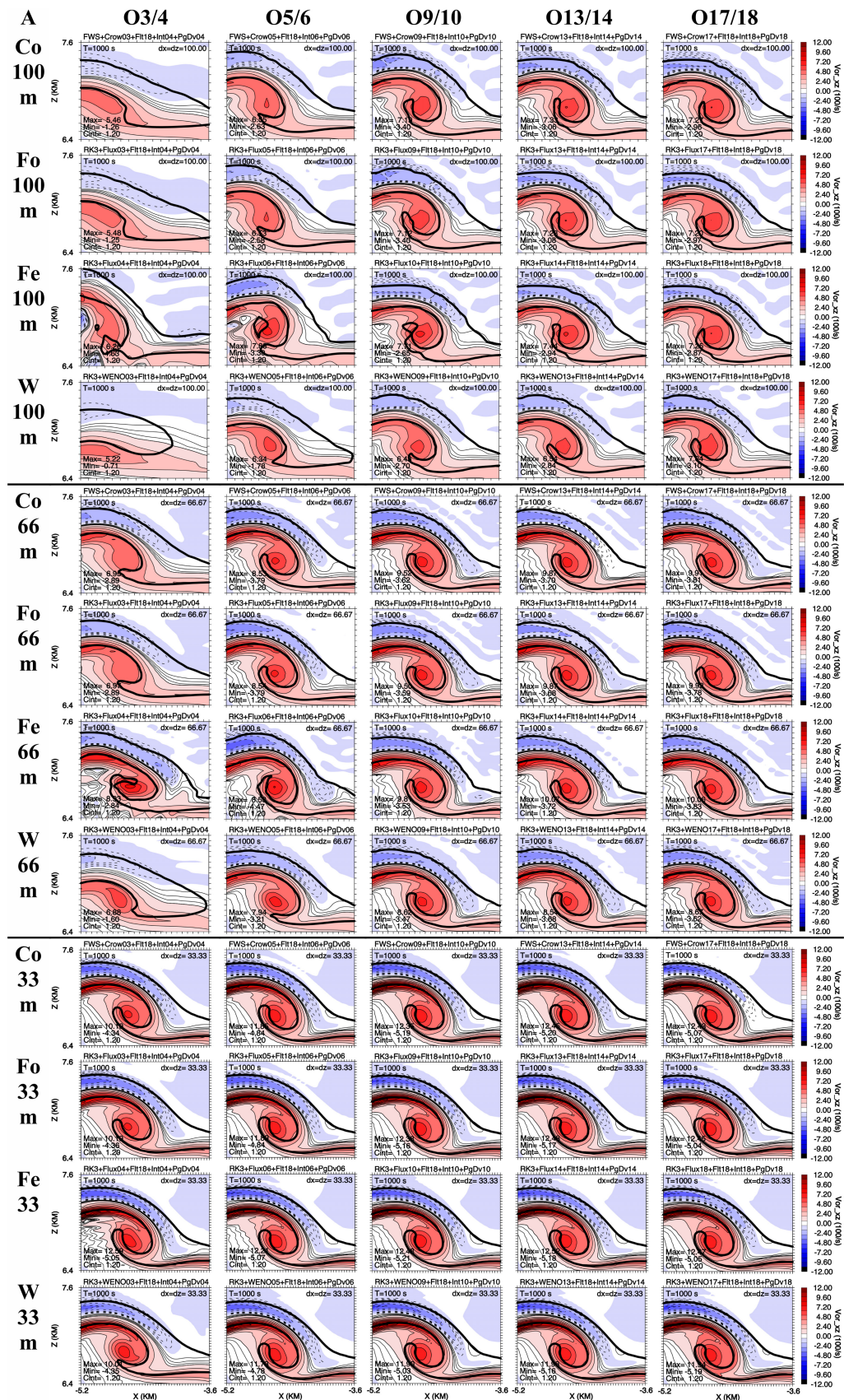


FIGURE 7 As in Figure 6, except for vorticity (100 s^{-1}). The bold solid line is the 0.2 K perturbation potential temperature contour of the simulation in the plot. [Colour figure can be viewed at wileyonlinelibrary.com]

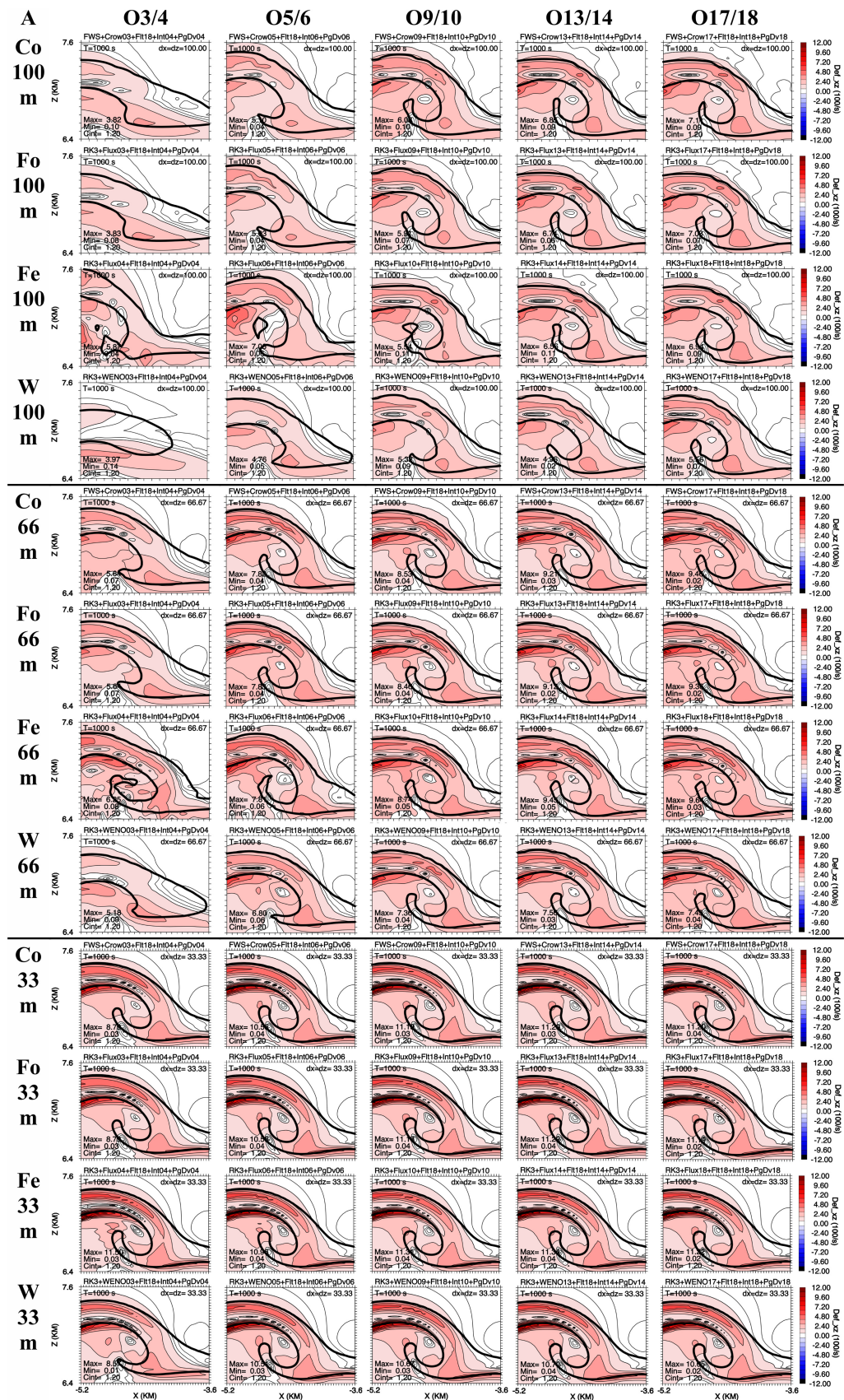


FIGURE 8 As in Figure 7, except for deformation (100 s⁻¹). The bold solid line is the 0.2 K perturbation potential temperature contour of the simulation in the plot. [Colour figure can be viewed at wileyonlinelibrary.com]

at best at $\sim O2$ except for some very high order and fine resolution solutions where convergence was $\sim O3$ and occasionally higher (Figure 2), with convergence rates slowly flattening at higher resolutions for $<O17/18$, but not for $O17/18$. This is similar to what $N21$ showed for nonlinear, shock-producing, 1D Euler simulations.

While many simulations were able to reasonably capture the resolvable and marginally resolved characteristics of the flow with $\Delta x = \Delta z = 100$ m (Figure 3) or 133.33 m (not shown), and appear fairly similar between schemes, among like-schemes, among like-order of accuracy, and especially among the odd order schemes (Figure 1 and Figures 3–8), as well as among the even $O10$, $O14$ and $O18$ schemes, the perturbation potential temperature differences fields (Figure 5) show some very large local differences, which were typically ~ 1 – 2 K and occasionally larger than ± 3 K. These errors probably owe to a combination of phase and amplitude errors, and numerical dispersion and dissipation along with aliasing, all of which might not be fully appreciated from visual examination. The largest errors were especially in and near the boundaries of the smaller (less resolved) upper rotor and near the front and back edge of the outward (leftward) propagating front beneath the upper rotor. Comparisons of maxima and minima of the velocity components (not shown) have differences of 8–10% between similar order schemes (e.g. $O17/18$), as high as 15% for a given scheme amongst all of the orders discussed, and an overall maximum difference of 15%. The differences in the pressure fields among the schemes were generally $<5\%$ (not shown).

Even order constant grid flux and even order constant grid flux Crowley schemes, especially the low order ($O4$ and $O6$) forms, have more prominent high frequency wave numerical noise, which can cause excitation of physical instabilities as the numerically induced high frequency waves are not well controlled. These types of errors can disrupt the evolution of the larger scale features and produce unphysical solutions, as well as exaggerated maxima, minima, etc. Importantly, the Crowley schemes have some advantage over the constant grid flux solutions in terms of reduced dispersion errors, though the Crowley schemes tend to have slightly more dissipation errors. Nevertheless, the $O14$ and $O18$ constant grid flux and constant grid flux Crowley schemes have some of the best objective error measures (objective errors for $\Delta x = \Delta z = 100$ m are tabulated in Table 3, while objective errors for $\Delta x = \Delta z = 100$, 66.67 and 33.33 m are also tabulated in Table 4 along with CPU timings which are discussed later), and these were very slightly better than $O13$ and $O17$ odd order schemes. In contrast, odd-order constant grid flux numerical approximations have much less obvious dispersion/phase and aliasing errors than even order schemes (especially for $<O10$ fluxes), appear

relatively free of numerical noise, and have the best overall visual performance and objective error measures for all orders.

Notice that the $O13$ – $O17$ WENO solutions using $\Delta x = \Delta z = 100$ m (Figure 3) tend to produce a perturbation in the potential temperature field on the top-left side of the interface, while none of the other solutions produce this perturbation. This same perturbation appeared in the non-viscous WENO colliding plume solutions described by $N21$, and appears to be associated with numerically accentuated shear and buoyancy gradients, both of which were already large, causing an unphysical feedback, based on the behaviour of the reference solution and WENO simulations with finer resolutions of $\Delta x = \Delta z = 25$, 33.33, 50 and 66.67 m for guidance, none of which have this perturbation. The objective measures (Figure 2; Table 3) show that error improvement stops and gets worse as order is increased from $O13$ to $O17$ for the 100 m WENO solutions, while all of the other schemes continue to have improved errors with increasing order. In contrast to the $>O5$ WENO solutions, as well as the other odd solutions with the non-WENO schemes, the $O3$ – $O5$ WENO solutions, and especially the $O3$ WENO solutions, appear overly smooth with significantly smaller amplitude maxima and minima (Figures 3–8). Moreover, the $O3$ – $O5$ WENO solutions (Figure 2) are not as accurate as the odd order flux scheme solutions either visually or with objective error measures. The damped $O3$ – $O5$ WENO solutions herein are consistent with the well-known issue of excessive damping of gradients with $O3$ – $O5$ WENO schemes documented by, for example, Latini *et al.* (2006) and Wang *et al.* (2021 WPM21). Though not shown for brevity, it is important to note that the WENO simulations show the well-known exceptional behaviour of preserving strong gradients both with and without artificial viscosity (eddy mixing and/or spatial filters), while the other schemes, especially the even order schemes, need spatial filtering.

Overall, considering all orders-of-accuracy and all resolutions tested, the results discussed for the case of no added mean wind (Set A) show that odd order constant grid flux schemes perform the best against the reference solution (as might be expected since the reference solution is obtained using the odd order constant grid flux scheme with $O17$, and 25 m). Additionally, the $O10$ – $O18$ even order constant grid flux schemes performed remarkably well for intermediate and finer grid resolutions ($\Delta x = \Delta z = 33.33$ – 100 m). However, the $O4$ – $O6$ even order constant grid flux solutions, and to a very slightly lesser degree the $O4$ – $O6$ Crowley schemes, produced solutions that were all very noisy and contaminated with significant dispersion and aliasing errors, the latter noticeable in the presence of prominent 3Δ waves, both visually identifiable

TABLE 3 RMS errors with four significant digits for potential temperature/kinetic energy per unit volume in simulation Sets A–H for $\Delta x = \Delta z = 100$ m simulations with errors computed using the O17, 25 m reference simulation.

	Schemes	O3/4	O5/6	O9/10	O13/14	O17/18
A	Co	0.1399/1.768	0.1064/1.302	0.08396/1.088	0.07378/1.024	0.07001/1.012
	Ce	0.1980/2.472	0.1352/1.439	0.08735/1.075	0.07347/1.001	0.06984/0.09552
	Fo	0.1420/1.811	0.1069/1.302	0.07862/1.035	0.07149/1.002	0.07037/1.050
	Fe	0.2106/2.623	0.1413/1.497	0.08670/1.058	0.07183/0.9846	0.07038/1.002
	W	0.1909/2.429	0.1200/1.527	0.08947/1.163	0.08698/1.130	0.1023/1.154
B	Co	0.2123/3.018	0.1983/2.587	0.2054/2.821	0.2084/2.854	0.2093/2.875
	Ce	0.2467/3.465	0.2225/3.045	0.2093/2.883	0.2083/2.873	0.2099/2.897
	Fo	0.2026/2.893	0.1811/2.698	0.1801/2.659	0.1803/2.680	0.1798/2.692
	Fe	0.2513/3.910	0.2289/3.323	0.1993/2.972	0.1850/2.758	0.1842/2.751
	W	0.2499/3.992	0.1838/2.700	0.1715/2.587	0.1739/2.622	0.1742/2.569
C	WR	0.1909/2.429	0.1299/1.642	0.1095/1.380	0.1029/1.283	0.09734/1.271
	WS	NA	NA	0.08055/1.137	0.08110/1.136	0.07697/1.077
D	WL c:c:17	0.1007/1.136	0.1013/1.144	0.1015/1.148	0.1023/1.155	0.1023/1.154
	WH17:17:c	0.1649/2.436	0.1217/1.548	0.09241/1.180	0.08866/1.136	0.1023/1.154
	WH P1c	0.1908/2.427	0.1199/1.527	0.08956/1.162	0.08707/1.131	0.1023/1.154
E	Fs Wv	0.1648/2.104	0.1102/1.424	0.08707/1.151	0.08363/1.098	0.08235/1.071
	Fv Ws	0.1711/2.072	0.1121/1.283	0.08226/1.035	0.07877/1.033	0.09121/1.061
F	Co2	0.1399/1.768	0.1064/1.302	0.08401/1.088	0.07380/1.024	0.07001/1.012
G	Hy	0.1918/2.421	0.1204/1.525	0.09058/1.171	0.08820/1.135	0.1002/1.147
	HS	NA	NA	0.08247/1.135	0.08315/1.171	0.07554/1.060
	H2S	NA	NA	0.08247/1.135	0.08315/1.171	0.07554/1.060
	Hs cv	0.1715/2.066	0.1123/1.293	0.08236/1.065	0.07909/1.053	0.08803/1.069
	Hv Cs	0.1640/2.078	0.1117/1.434	0.09012/1.180	0.08500/1.107	0.08374/1.064
H	Fv s17	0.1452/1.820	0.1109/1.318	0.08671/1.140	0.08113/1.144	0.07037/1.050
	Fs v17	0.1143/1.372	0.08570/1.060	0.07148/0.9861	0.07029/1.006	0.07037/1.050

Note: The top row indicates odd/even order solutions from O3/4–17/18.

Abbreviations: **Co** = odd order upwind-biased constant grid flux Crowley; **Ce** = even order constant grid flux Crowley; **Fo** = upwind-biased odd order constant grid flux; **Fe** = even order constant grid flux; **W** = WENO flux; **WS** = W with sine-based smoothness indicators; **WR** = W with smoothness indicator power given by $p = R$, where $O = 2R - 1$; **WL c:c:17** = O3, 5, 9 or 13 W for stages one and two of RK3, and O17 W for stage three of RK3; **WH** = (17:17:c) = O17 W for stages one and two of RK3, and O3, 5, 9 or 13 W for stage three of RK3; **WH P1c** = (17:17:c) = O17 W for stages one and two of RK3, and O3, 5, 9 or 13 W for stage three of RK3 with comparable order interpolations and pressure gradient/divergence; **Ws Fv** = W for scalars and Fo for velocities/pressure; **Fs Wv** = Fo for scalars and W for velocities/pressure; **Co2** = O3, 5, 9, 13 or 17 Co with $N = 2$ derivatives in place of N = order of Crowley scheme; **Hy** = hybrid WENO/Crowley flux; **HS** = hybrid WENO/Crowley flux with sine-based smoothness indicators ($p = 1$); **H2S** = hybrid W for scalars and Co with $N = 2$ derivatives in place of N = order of Crowley scheme; **Hs Cv** = hybrid W for scalars and Co for velocities/pressure; **Hv Cs** = hybrid W for velocities/pressure and Co for scalars; **Fv s17** = lower order Fo (O3, 5, 9 or 13) for velocities/pressure and O17 Fo for scalars; and **Fs v17** = lower order Fo (O3, 5, 9 or 13) for scalars and O17 Fo for velocities/pressure. NA = not available. The bold numbers are the four lowest RMS errors for each set.

and in power spectra of the velocity components, KE, vorticity, and potential temperature (not shown).

Visual inspection of the solutions in Figure 1 and Figures 3–8 shows that increasing the order of accuracy of approximations used to make the solutions by two to four orders is roughly comparable to making the resolution 1.5–3 times finer, consistent with Shi *et al.* (2003),

Latini *et al.* (2006) and SWK23. All O9–17 solutions with $\Delta x = \Delta z = 50$ m (not shown) and 66.67 m appear nearly as good visually and perhaps better than the O3–5 solutions made with $\Delta x = \Delta z = 33.33$ m (factor of 1.5–2; in particular, see difference fields between 25 m reference and test solutions for perturbation potential temperature in Figure 5).

TABLE 4 CPU times (s) for odd and even order Crowley flux (schemes **Co** and **Ce**), odd and even order flux (schemes **Fo** and **Fe**), and odd order WENO flux (scheme **W**), using 100, 66.67 and 33.33 m and time $t = 31.25$ s (100, 200 and 300 steps), along with RMS errors for perturbation potential temperature (top number in each cell) and kinetic energy per unit volume (bottom number in each cell).

4A CPU times and RMS errors using a resolution of 100 m										
100 m scheme	O3/4 CPU	O3/4 RMS	O5/6 CPU	O5/6 RMS	O9/10 CPU	O9/10 RMS	O13/14 CPU	O13/14 RMS	O17/18 CPU	O17/18 RMS
Co	1.81/1.00	0.1399	2.48/1.37	0.1064	4.53/2.50	0.08396	5.56/3.07	0.07378	6.31/3.49	0.07001
	20.8/1.00	1.768	21.2/1.02	1.302	23.9/1.15	1.088	25.2/1.21	1.024	25.3/1.22	1.012
Ce	1.59/1.00	0.1980	2.37/1.49	0.1352	3.36/2.11	0.08735	4.38/2.75	0.07347	5.21/3.28	0.06984
	18.4/1.00	2.472	19.6/1.07	1.439	21.0/1.14	1.075	22.0/1.20	1.001	22.0/1.20	0.9952
Fo	1.38/1.00	0.142	2.22/1.61	0.1069	3.12/2.26	0.07862	3.91/2.83	0.07149	4.96/3.59	0.07037
	27.0/1.00	1.811	28.5/1.06	1.302	30.1/1.11	1.035	30.5/1.13	1.002	31.9/1.18	1.017
Fe	1.28/1.00	0.2106	2.02/1.57	0.1413	2.91/2.23	0.08670	3.90/3.04	0.07183	4.87/3.80	0.07377
	19.0/1.00	2.623	20.1/1.06	1.497	20.6/1.08	1.058	21.9/1.15	0.9846	23.3/1.23	1.003
W	NA	0.1909	NA	0.1200	NA	0.08975	NA	0.08698	NA	0.1023
	44.8/1.00	2.429	52.0/1.16	1.527	56.4/1.26	1.163	61.3/1.37	1.130	67.4/1.50	1.154

4B CPU times and RMS errors as in Table 4A, except using a resolution of 66.67 m										
66 m scheme	O3/4 CPU	O3/4 RMS	O5/6 CPU	O5/6 RMS	O9/10 CPU	O9/10 RMS	O13/14 CPU	O13/14 RMS	O17/18 CPU	O17/18 RMS
Co	5.79/1.00	0.08712	8.13/1.34	0.05272	14.7/2.38	0.04601	17.7/2.80	0.04318	21.0/3.62	0.03923
	56.3/1.00	1.027	58.8/1.04	0.7156	65.5/1.16	0.6818	70.5/1.25	0.6605	76.1/1.35	0.6025
Ce	4.94/1.00	0.09374	7.29/1.48	0.06561	11.2/2.27	0.04721	14.2/2.87	0.04245	17.0/3.44	0.03915
	50.4/1.00	1.0271	53.8/1.07	0.8279	58.5/1.16	0.6800	62.3/1.24	0.6386	63.9/1.27	0.5873
Fo	3.93/1.00	0.08788	6.68/1.70	0.04953	9.67/2.46	0.0403	12.5/3.18	0.03884	15.8/4.02	0.03981
	76.3/1.00	1.032	80.8/1.06	0.6744	88.3/1.16	0.6150	90.1/1.18	0.6001	95.4/1.25	0.5705
Fe	3.84/1.00	0.09472	5.83/1.82	0.06503	9.53/2.48	0.04409	12.5/3.26	0.03973	15.4/4.01	0.03871
	49.5/1.00	1.063	53.5/1.08	0.7991	57.1/1.15	0.6364	61.3/1.24	0.5988	64.7/1.31	0.5674
W	NA	0.1383	NA	0.06915	NA	0.04632	NA	0.04628	NA	0.04512
	133.2/1.00	1.618	172.5/1.30	0.9237	183.2/1.38	0.6768	200.7/1.51	0.6492	225.3/1.69	0.6126

TABLE 4 (Continued)

4C CPU times and RMS errors as in Table 4A, except using a resolution of 33.33 m										
33 m scheme	O3/4 CPU	O3/4 RMS	O5/6 CPU	O5/6 RMS	O9/10 CPU	O9/10 RMS	O13/14 CPU	O13/14 RMS	O17/18 CPU	O17/18 RMS
Co	45.0/ 1.00	0.02868	62.4/ 1.39	0.02401	108.3/ 2.41	0.02849	131.1/ 2.91	0.02369	150.9/ 3.35	0.0115
	364.8/ 1.00	0.3777	381.3/ 1.05	0.3125	430.5/ 1.18	0.3503	461.4/ 1.26	0.2962	483.6/ 1.33	0.1639
Ce	36.0/ 1.00	0.02577	55.0/ 1.53	0.02441	81.0/ 2.25	0.02432	104.7/ 2.76	0.01839	124.8/ 3.47	0.00885
	316.8/ 1.00	0.3580	339.0/ 1.07	0.3146		0.3077	391.8/ 1.24	0.2365	414.3/ 1.31	0.1355
Fo	28.0/ 1.00	0.02581	48.1/ 1.72	0.02026	69.9/ 2.50	0.02035	92.1/ 3.30	0.01576	117.0/ 4.19	0.00755
	459.6/ 1.00	0.3421	493.2/ 1.07	0.2674	528.9/ 1.15	0.2610	564.9/ 1.23	0.2100	604.5/ 1.32	0.1163
Fe	28.1/ 1.00	0.02233	47.7/ 1.70	0.02070	69.0/ 2.46	0.02064	92.1/ 3.23	0.01589	114.9/ 4.09	0.00758
	311.4/ 1.00	0.3158	343.5/ 1.10	0.2702		0.2634	380.7/ 1.22	0.2110	404.4/ 1.30	0.1165
W	NA	0.05527	NA	0.01941	NA	0.02072	NA	0.01526	NA	0.00768
	1,088.4/ 1.00	0.6198	1,548.0/ 1.42	0.2487	1,692.7/ 1.56	0.2646	1860.3/ 1.71	0.2116	2085.9/ 1.92	0.1234

Note: Top values for each scheme and order are CPU times for only the flux stencil + pressure gradient stencil + divergence stencil + interpolation stencil calculations and next to the CPU time in bold is the ratio to the lowest order scheme (O3/4) in the row. The second value for each scheme and order are CPU time for only total advection + total small step + total buoyancy and next to the CPU time in bold is the ratio to the lowest order scheme (O3/4) in the row. The CPU times for the O18 filter (SGS turbulence) are ~0.1, 0.3 and 0.9 s (7, 14 and 38 s) for Crowley simulations, and 0.2, 0.4, 1.4 s (11, 21, 57 s) for RK3 solutions (both odd and even flux and odd WENO) using 100, 66.66 and 33.33 m, respectively. Note with a constant Courant number, 66.66 and 33.33 m resolution solutions take 1.5 and 3 times more time steps than the 100 m resolution solutions. (The flux stencil CPU times were not collected for the WENO solutions and labelled NA or not available; however, the total advection + total small step + total buoyancy time was so row two in each cell was available.)

The computational cost is approximated for each scheme from a theoretical perspective to avoid computer/compiler dependence as total floating-point operations (FPO) per grid point per time step for the three-stage RK3 mode-split time integrations using two, three and six fast mode small time steps per slow-mode time step, for stages one, two and three, respectively times the number of grid points times the number of time steps (Figure 9). The use of order of accuracy preserving interpolations and pressure gradient/divergence calculations results in FPO numbers greater than those compared to using O2 interpolations and pressure gradient/divergence calculations as is traditionally done in most atmospheric models. Overall accuracy does not seem to be degraded if $\geq O4$ is used for the interpolations and pressure gradient/divergence calculations, but is for O2 (SWK23). Importantly, the use of O4 for the interpolations and pressure gradient/divergence calculations results in many fewer FPOs compared to use of comparable order of accuracy for these calculations (SWK23). Note the approximate linear increase with order of FPOs per grid point per time step for the flux and Crowley schemes, cubic increase for WENO schemes, and

quadratic increase for WENO-Sine solutions (discussed in Section 3.4.2). The total FPOs in the graphs of Figure 10 were all normalised by the $\Delta x = \Delta z = 166.67$ m O4 constant grid flux scheme FPO value (the lowest value of all schemes and resolutions considered) and are based on keeping the Courant number constant, and provides the basis which provides a relative computational cost for each scheme using with O3/4, 5/6, 9/10, 13/14 and 17/18 order numerical approximations and resolutions of $\Delta x = \Delta z = 25, 33.33, 50, 66.67, 133.33$ and 166.67 m, relative to the RMS errors for perturbation potential temperature and KE (Figure 10). Use of a time step based on the stable CFL rather than a constant Courant number becomes more complex, especially for the lower order ($\leq O5/6$) solutions. First, temporal truncation errors tend to increase with longer time steps for this problem (e.g. SWK23). Second, the solutions with longer time steps required fewer total computations, which might offset the impact of accumulated temporal errors.

Comparisons of computational costs based on FPOs versus potential temperature and KE RMS errors for all solutions is best seen graphically, which shows that the

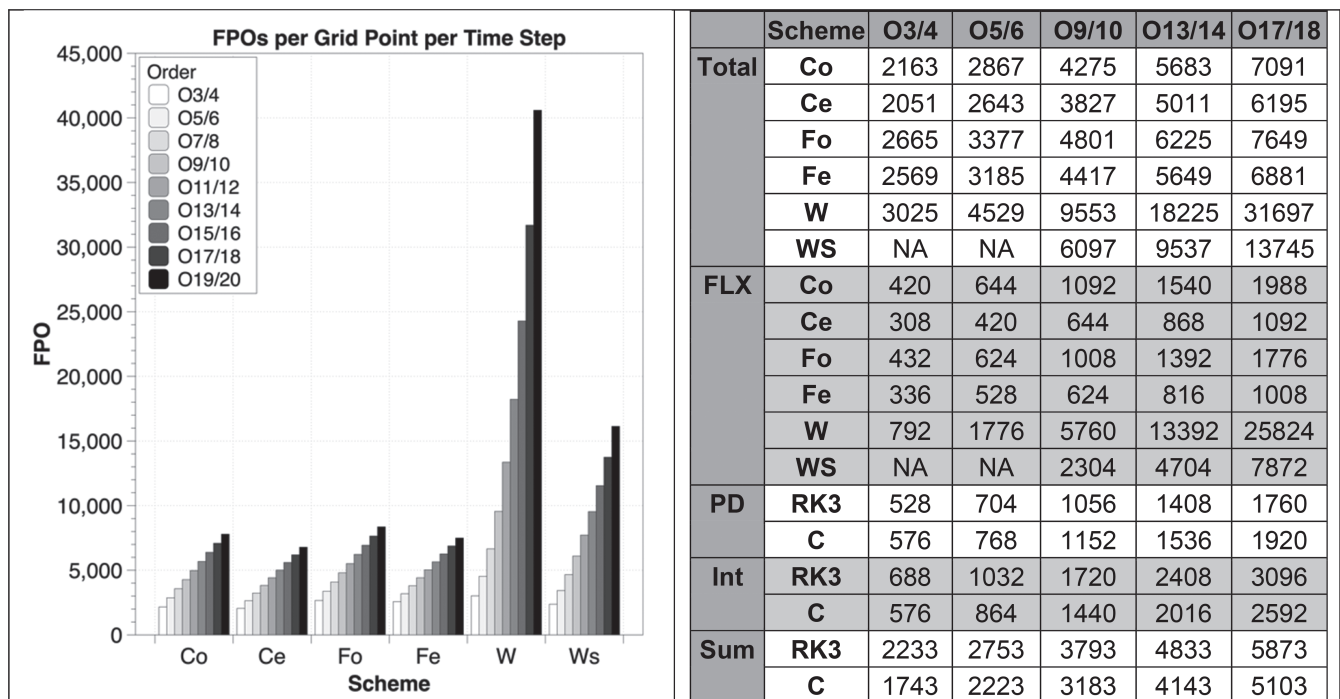


FIGURE 9 Set A approximate (Total) Floating-Point Operations (FPOs) per grid point per time step for each scheme (left chart), constant grid flux Crowley (Co = odd; Ce = even), constant grid flux (Fo = odd; Fe = even), WENO flux (W), and WENO with sine wave-based smoothness indicator (WS; for $R \geq 4$, which is $\geq O7$, notes values for O3 and O5 WS are theoretical). The table (right) includes the approximate total floating-point operations (FPO) per grid point per time step (Total) and the FPO for advection (FLX). The bottom six rows of the table contain the approximate FPO for WS02 forward mode-split Crowley (C) and mode-split RK3 time integrations for pressure gradient/divergence (PD), all non-flux interpolations (Int), and the sum (Sum) of FPOs for PD, Int, buoyancy, and filter terms. The FPO values for Sum of PD, Int, buoyancy, and filter terms using O2 and O4 numerical approximations are 1,713 and 2,233 for mode-split RK3, and 1,263 and 1,743 for WS02 forward mode-split Crowley, respectively.

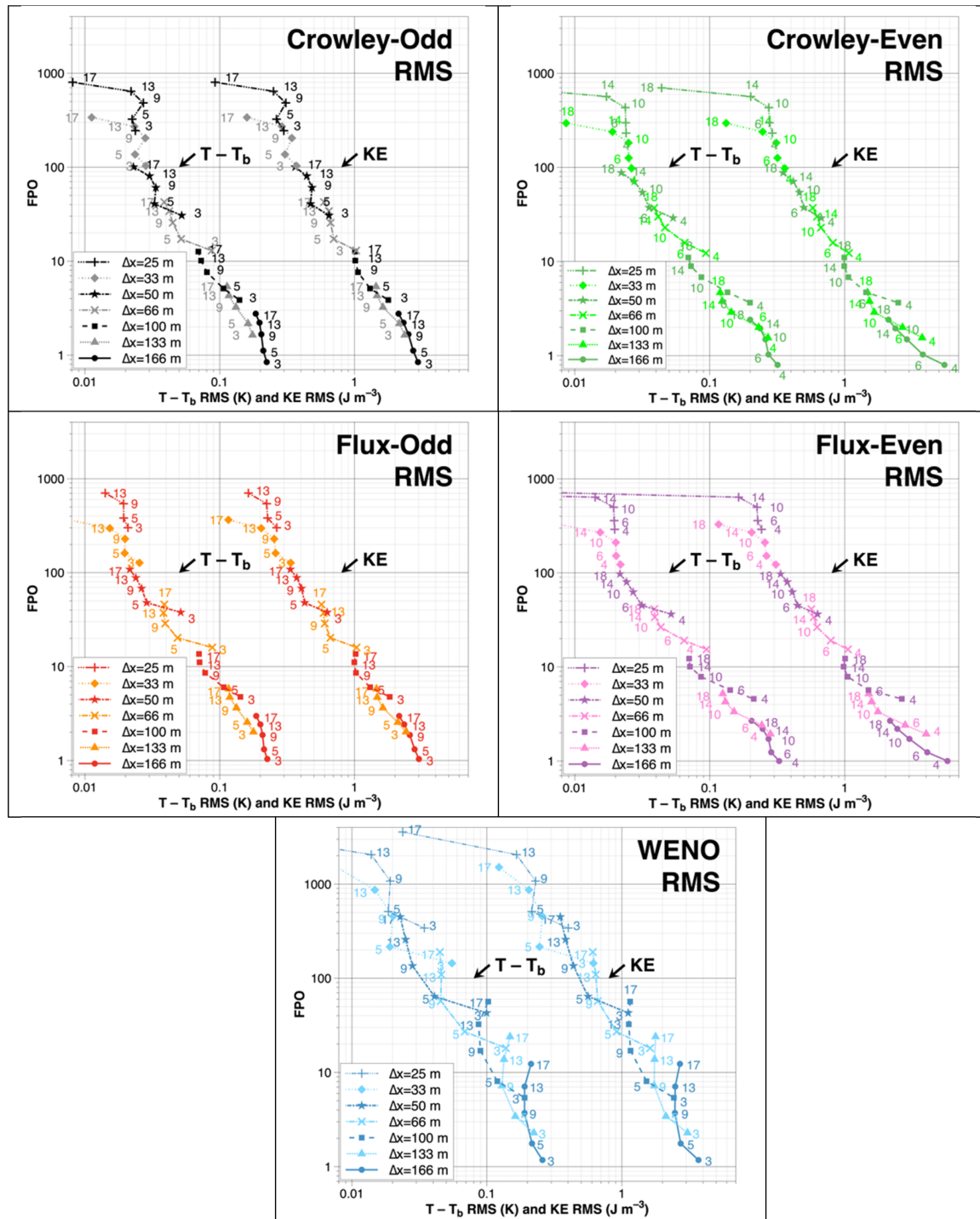


FIGURE 10 Set A log-log charts of the computational cost (total Floating-Point Operations FPO) versus Root Mean Square errors (RMS) for Perturbation potential temperature ($T - T_b$; K; left-most curve cluster in each panel) and Kinetic Energy (KE; $J m^{-3}$; right-most curve cluster in each panel) calculated against the upwind-biased constant grid flux O17, 25 m reference solution for the odd/even order O3/4, 5/6, 9/10, 13/14 and 17/18 upwind-biased/centred Crowley constant grid flux (Co = odd, upper left; Ce = even, upper right) odd/even order O3/4, 5/6, 9/10, 13/14 and 17/18 upwind-biased/centred constant grid flux (Fo = odd, middle left; Fe = even, middle right) and odd order O3, 5, 9, 13 and 17 WENO flux (W; bottom) schemes comparable order interpolations and pressure gradient/divergence, O18 spatial filter, same Courant number C , and constant eddy mixing coefficient of $K_m = 10 m^2 s^{-1}$ for grid resolutions of $\Delta x = \Delta z = 25, 33.33, 50, 66.67, 100, 133.33$ and 166.67 m (legend). The total FPO values (for all grid points and all time steps, i.e. the entire simulation) are all normalised by the FPO value for the centred constant grid flux O4 $\Delta x = \Delta z = 166.67$ m simulation for comparison purposes. [Colour figure can be viewed at wileyonlinelibrary.com]

solutions with the best objective errors for the computational cost are solutions made at the finest resolutions with highest even order flux, odd order flux (Figure 10), even order Crowley solutions, while WENO solutions had significantly larger computation costs (Figure 10). Clearly, except at the highest orders and high resolutions, most schemes are not cost-effective based on the use of the theoretical FPOs. Using near the maximum stable CFL only worsens the cost-effectiveness for each scheme. The lack of cost-effectiveness seems to be associated, at least in part, with the diffusion-limited nature of the problem and temporal errors, especially temporal errors with the filter, as discussed in SWK23.

Fortunately, efficient computer cache use, which can be machine dependent, can allow for significant cost-effectiveness with higher order schemes as described by, for example, Balsara and Shu (2000) and Shi *et al.* (2003), who showed computational costs based on CPU times were up to two or more times less than costs estimated from FPOs. In this study, attempts at careful programming resulted in better use of faster computer caches and reduced cost for all schemes compared to expectations based on FPOs. Values for the CPU times for each scheme order along with RMS errors for perturbation potential temperature (top RMS value for each order) and KE (bottom RMS value for each order) are presented for 100, 66.67 and 33.33 m solutions in Table 4. The first CPU value in the for each scheme order is CPU time for only the flux stencil + pressure gradient stencil + divergence stencil + interpolation stencil calculations and next to this CPU time in bold is its ratio to the lowest order scheme (O3/4) in the row. The second CPU value for each scheme order is CPU time for only total advection + total small step + total buoyancy and next to this CPU time in bold is its the ratio to the lowest order scheme (O3/4) in the row. The CPU for the SGS turbulent flux and spatial filter calculations are the same amongst Crowley solutions and same amongst RK3 solutions for any given resolution and included in the caption of Table 4. Efficient computer cache use, for example using the 100 m odd flux simulations, resulted in the ratio of the CPU time for O17 to O3 stencil calculations to be roughly only ~ 3.6 , when theoretically using FPOs the ratio would be ~ 6.6 (note the flux FPOs in Figure 9 included all calculations for fluxes, where in contrast only the stencil calculations were considered for this discussion). All calculations, including overhead calculations (e.g. dt/dx , map factors, density in the flux divergence term, etc.) needed to update dependent variables with fluxes, pressure gradient, and divergence, are significant, similar among the Crowley time integrations, similar among the RK3 time integrations, and are included in the second number in each table cell to help show why high order solutions do not dramatically

increase total CPU time in comparison to much lower order solutions. In another comparison, the O17 WENO flux solution CPU times (Table 4, second number), which were dominated by the flux calculations (84%–93% for O3–17 WENO fluxes, respectively), use only about ~ 1.5 – 2 times more CPU time (domain size dependent) than O3 WENO solutions, in contrast to using FPOs, for which the O17 WENO solutions could be expected to use ~ 10 times more CPU time than O3 WENO solutions. This made the WENO schemes much more attractive in terms of CPU time use compared to what could be expected using theoretical FPOs. The results in Table 4 also show that the use of CPU times rather than FPOs to estimate cost-effectiveness allows some higher order schemes to be more competitive, at least visually, and not much more CPU compared to lower order schemes. Finally, while use of higher order numerical approximations, at least for the colliding plume problem, is not always cost-effective, higher order numerical approximations can provide more accurate to much more accurate solutions when resolution is not changed, or cannot be changed for reasons such as limits associated with available computer memory.

3.3 | Comparisons of solutions with an added mean wind of $-20 \text{ m}\cdot\text{s}^{-1}$ (Set B)

Additional simulations, with an added mean wind of $U_t = -20 \text{ m}\cdot\text{s}^{-1}$, were compared at $t = 1,000 \text{ s}$ for all schemes made with comparably high order interpolation and pressure gradient/divergence approximations, same O18 spatial filter, same Courant number C , and $\Delta x = \Delta z = 25$ – 166.67 m . Use of the added mean wind proved to be more of a challenge for all schemes, as seen in the perturbation potential temperature fields (Figure 11). As with the solutions without the added mean wind, additional comparisons were made between solutions at $t = 1,000 \text{ s}$ in the vicinity of the marginally resolved upper rotor where the largest errors generally occurred for the odd order Crowley, odd and even order constant grid flux, and WENO flux schemes, with comparable order interpolations and pressure gradient/divergence, same O18 filter, same Courant number C , and resolutions of $\Delta x = \Delta z = 33.33$, 66.67 and 100.00 m for perturbation potential temperature (Figure 12) and kinetic energy per unit volume (Figure 13).

The odd order constant grid flux, odd order constant grid flux Crowley, and WENO flux schemes produced the better solutions than the even order constant grid flux and even order Crowley schemes for all orders-of-accuracy, in terms of rotor shape preservation and amplitude and phase errors, when compared to solutions without an added

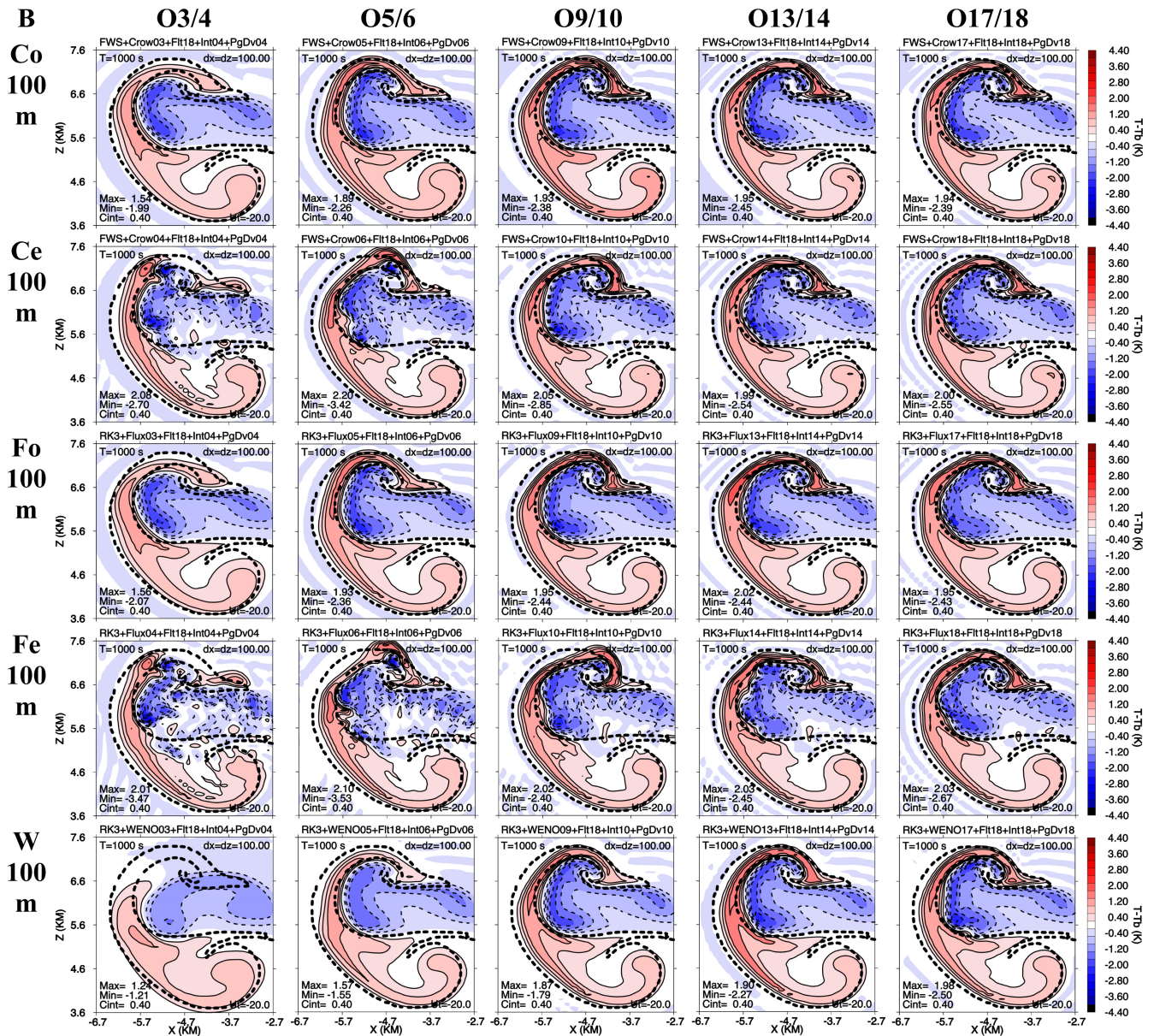


FIGURE 11 As in Figure 3, except for Set B simulations (i.e., with an added mean wind of $U_t = -20 \text{ m s}^{-1}$) perturbation potential temperature ($T - T_b$; K). The bold dashed line is the 0.2 K perturbation potential temperature contour of the upwind-biased constant grid flux O17, 25 m reference solution interpolated to each grid. [Colour figure can be viewed at wileyonlinelibrary.com]

wind and to the reference solution from the simulations without the added wind (theoretically, the solution should be the same with and without an added mean wind due to Galilean invariance; however, the mean wind adds a further challenge to the numerical schemes not present in the no-wind simulations). Unsurprisingly, the phase errors, which are enhanced by strong advection from the added mean wind, were minimised with the higher order approximations. The degree of improvements, which are notable and continued up to O17/18, were somewhat unexpected. Some minor loss in symmetry in the rotor shape and flow fields (features on left side versus right side of domain)

occurred with all schemes, especially with the even order schemes and spatial resolutions of 100, 66.67 and 33.33 m (all schemes and all orders are shown in Supporting Information S4) for the simulations with the added mean wind owing to variations in dispersion and phase errors in the parts of the solutions moving with and opposing the flow, especially for lower order even flux schemes. The even order Crowley schemes produced less asymmetries than even order flux schemes, while the WENO schemes produced the least asymmetries at any order for any accuracy at any given resolution compared to the odd/even Crowley and odd/even flux schemes. The asymmetries decreased

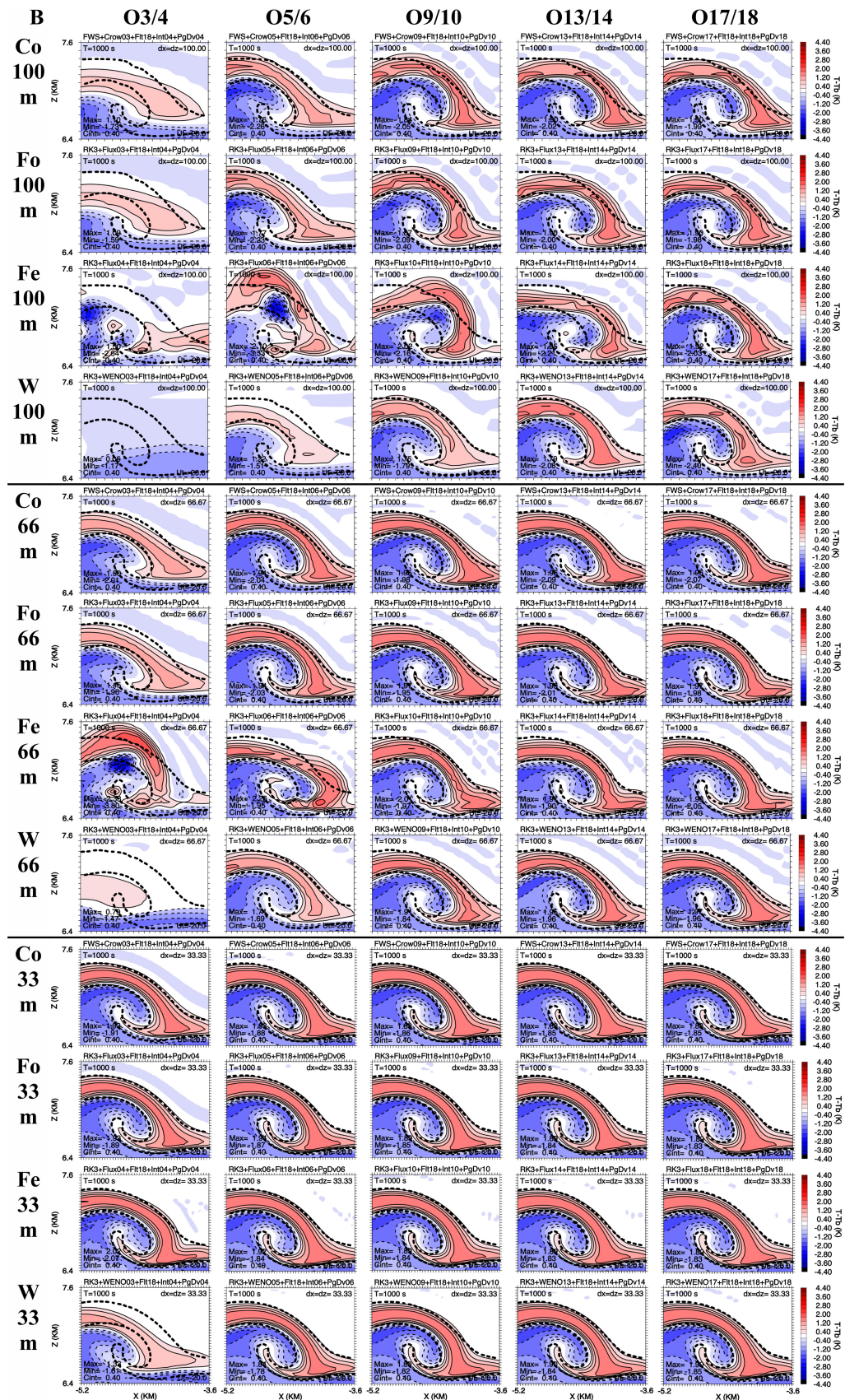


FIGURE 12 As in Figure 4, except for Set B simulations (i.e. with an added mean wind of $U_t = -20 \text{ m s}^{-1}$). Perturbation potential temperature ($T - T_b$; K). The bold dashed line is the 0.2 K perturbation potential temperature contour of the upwind-biased constant grid flux O17, 25 m reference solution interpolated to the grid. [Colour figure can be viewed at wileyonlinelibrary.com]

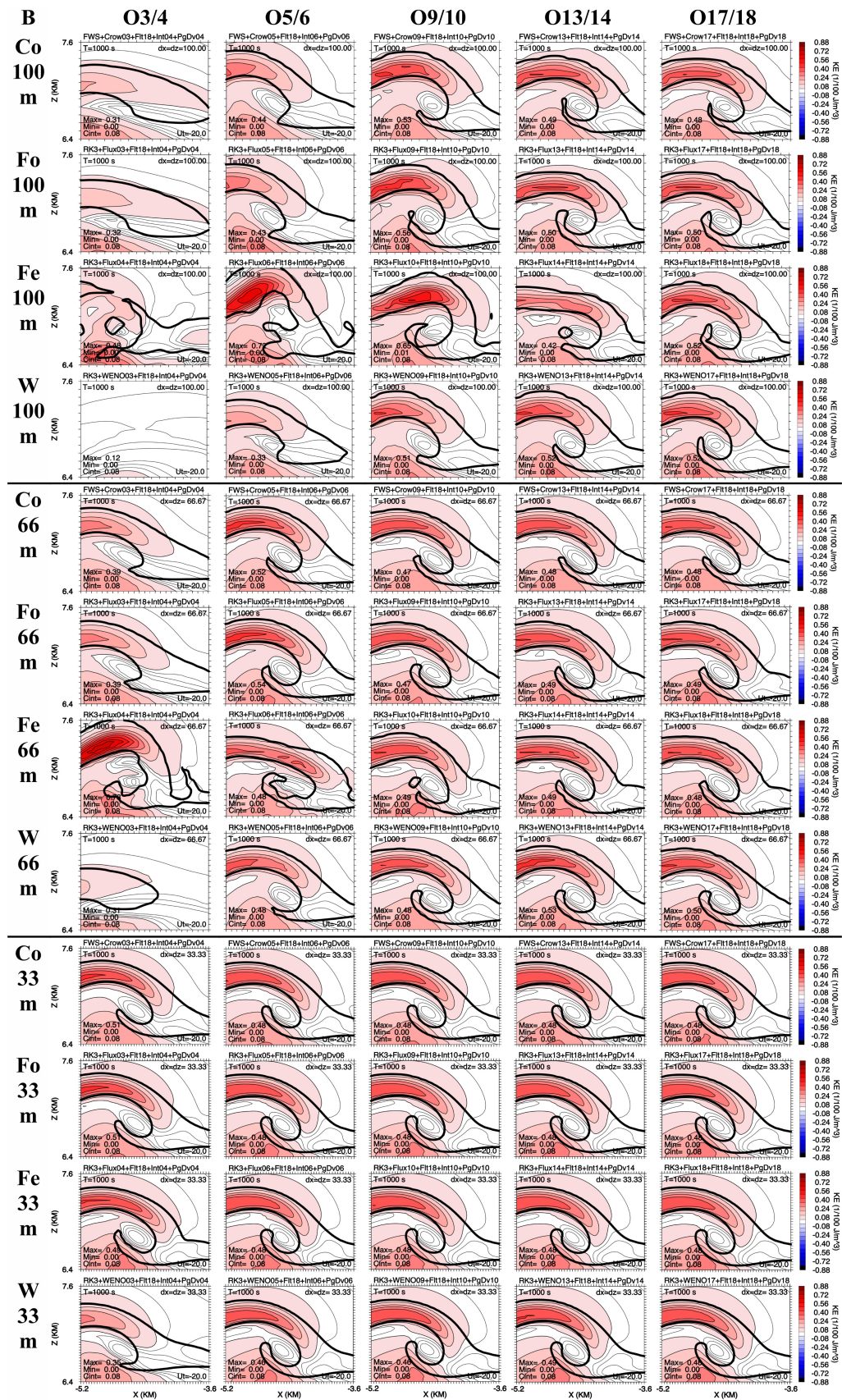


FIGURE 13 As in Figure 6, except for Set B simulations (i.e. with an added mean wind $U_t = -20 \text{ m s}^{-1}$). Kinetic Energy per unit volume (KE; $1/100 \text{ J} \cdot \text{m}^{-3}$). The bold solid line is the 0.2 K perturbation potential temperature contour of the simulation in the plot. [Colour figure can be viewed at wileyonlinelibrary.com]

with both increasing scheme orders and spatial resolutions but were still present for spatial resolutions of 33.33 m; however, they were barely visible (Supporting Information S4).

Interestingly, the apparent phase errors (based on visual assessment of the placement of the leading potential temperature front (relative to the reference solution, dashed contour) are the smallest in the O17 WENO solutions made with $\Delta x = \Delta z = 100$ m (Figure 11) compared to all of the other solutions for this resolution regardless of the order of accuracy with which they were made. Additionally, the O5, 9, 13 and 17 WENO solutions also tend to have the lowest RMS errors (Table 3) for potential temperature and KE among the schemes for Set B. However, the O3–5 (and to a lesser degree O9) WENO solutions with the added mean wind have the worst visual appearance, followed by the O3 and O5 Crowley solutions, even at finer resolutions of $\Delta x = \Delta z = 50$ and 33.33 ... m (not shown). The solutions made with even order flux finite difference schemes, and to a slightly lesser extent the even order Crowley schemes, were adversely affected by dispersion/phase and aliasing errors, especially those with <O10 numerical approximations, and much more so than the odd order scheme solutions. Additional spatial filtering (factor of 10 or more, higher) was needed with lower order even-centred constant grid flux schemes to control adverse dispersion and aliasing etc. errors (not shown) enough to make them as visually free of numerical noise as the odd order solutions. However, increasing filtering strength can adversely affect the overall accuracy, especially when evaluated in terms of amplitude error. In summary, the results with the added mean wind simulations showed that the highest order odd order schemes as well as the very highest order (\geq O9) even order schemes, were remarkably accurate and had minimal numerical noise for the case with an added mean wind.

3.4 | Constant grid, Crowley, and WENO flux advection scheme hybrids and variations

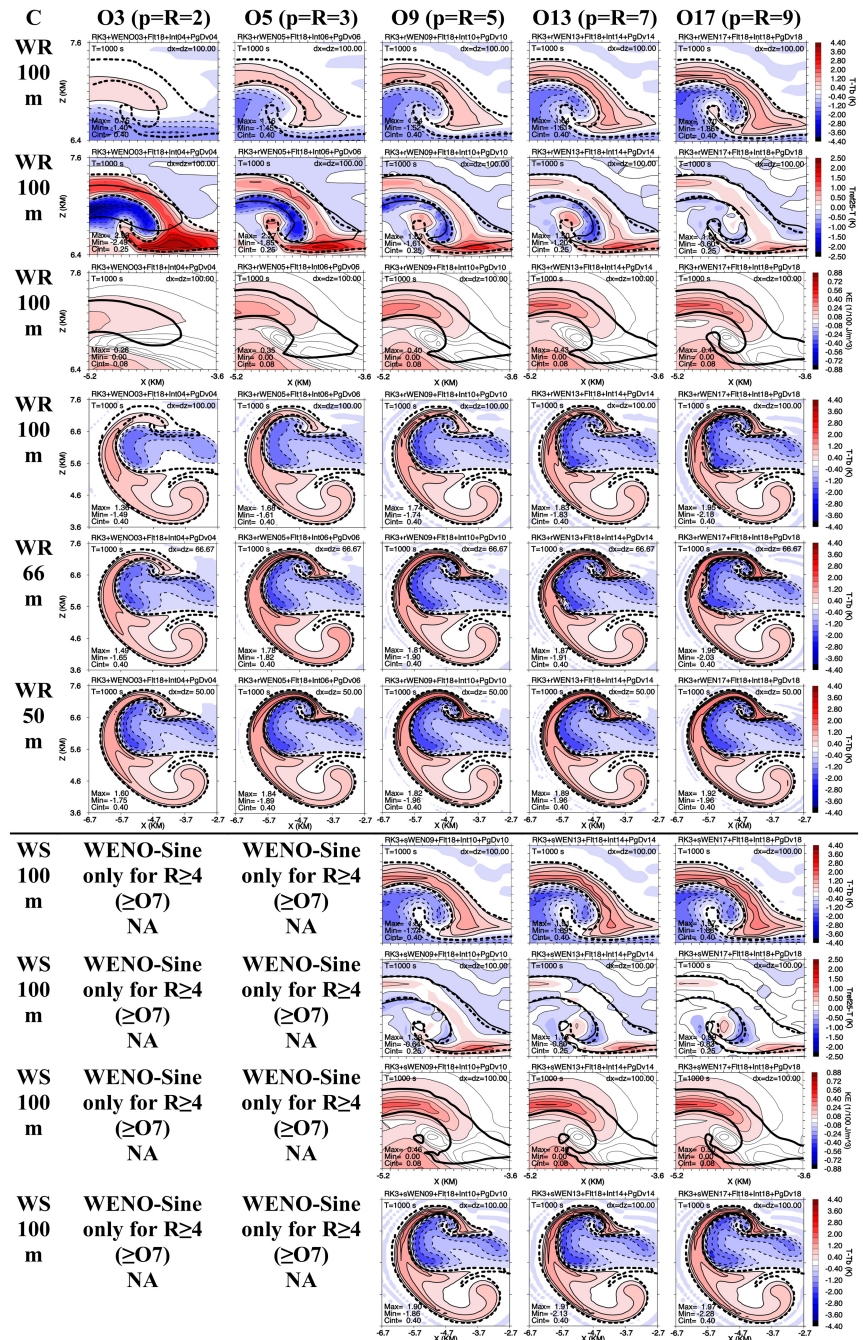
Several variations of odd order versions of constant grid, Crowley, and WENO flux schemes are evaluated next, as are various hybrids of these schemes, including a hybrid-WENO/Crowley scheme. Additionally, the WENO flux schemes, integrated with three-stage O3 RK3 time integration schemes, slowly continue to gain use in the atmospheric sciences. Given the high computational cost of numerical weather models, WENO and other schemes sometimes have been used with “short-cuts” to improve efficiency. However, the evaluation of the impact of any detriment to the scheme accuracy associated

with some of these implementation practices to improve computational efficiency has not always been demonstrated and/or documented for either linear or nonlinear atmospheric problems. The impacts of some of these implementations are presented in Sets C–H using $\Delta x = \Delta z = 100$ m resolution.

3.4.1 | WENO smoothness indicator power (Set C)

Gerolymos *et al.* (2009) showed examples of WENO solutions with up to O17, in which the WENO scheme smoothness indicator exponent parameter were given by $p = R$ (denoted as WR on plots), where order of accuracy $O = 2R - 1$, rather than using the traditional value of $p = 2$ (JS96; BS00; G09). (Note $p = 2$ for both O3 WR and O3 W.) Briefly, the O5–17 WENO flux solutions shown by G09 made using a value of $p = R$ were generally more monotonic, and more accurately captured the solutions in regions of very sharp boundaries/shocks for linear and nonlinear 1D problems compared to solutions made with $p = 2$. Comparisons of examples of WENO flux scheme solutions presented herein with the smoothness indicator exponent parameter given by $p = R$ (hereafter denoted as WR), instead of the traditional value of $p = 2$ (e.g. JS96; S97), and $\Delta x = \Delta z = 100$ m resolution, showed that the perturbation potential temperature field maxima and minima in the for O5, 9, 13 and 17 WR solutions did not overshoot values (e.g. were more monotonic) found in the reference solution. In contrast, for example, the perturbation potential temperatures maxima and minima in the O17, 100 m solutions made using of $p = 2$ (the worse-case) by 4.7 and 23.1%, respectively. These percents decreased in the O17, 66.67 m (50 m) resolution WENO flux solutions ($p = 2$) to 2.6% (1.6%) for perturbation potential temperature maxima, with no overshoots for the minima for either 66.67 or 50 m. Minimising overshoots and better monotonic behaviour by using $p = R$ was one of the defining impacts shown and discussed by G09. However, RMS errors were somewhat degraded for O5, 9 and 13 WR perturbation potential temperature and KE solutions herein using $p = R$ (Figure 14 rows one–three, WR, zoomed as in Figures 4–8; Table 3), although somewhat improved for O17 WR solutions, as compared to WENO with $p = 2$ (see Figures 4–6). It seems that using $p = R$ may have overdamped the solutions at 100 m resolutions resulting in larger RMS errors. Finer resolution solutions (e.g. $\Delta x = \Delta z = 66.67$ and 50 m) made using $p = R$ (Figure 14 rows five–six as in Figure 3) showed somewhat less damped solutions compared to solutions made using 100 m resolution and $p = R$ (Figure 14 row four as in Figure 3), with no overshooting maxima and minima of

FIGURE 14 Set C perturbation potential temperature ($T - T_b$; K; rows 1, 4, 5, 6, 7 and 10), difference between reference and test solution potential temperature ($T_{\text{Ref}} - T$; K; rows two and eight), and Kinetic Energy per unit volume (KE; $1/100 \text{ J} \cdot \text{m}^{-3}$; rows three and nine) fields at $t = 1,000 \text{ s}$ made with grid resolution of $\Delta x = \Delta z = 100 \text{ m}$, with O3, 5, 9, 13 and 17 WENO-R (WR) and O9, 13 and 17 WENO-Sine (WS) flux schemes, comparable order interpolations and pressure gradient/divergence, O18 spatial filter, same Courant number C , and constant eddy mixing coefficient of $K_m = 10 \text{ m}^2 \cdot \text{s}^{-1}$. The top six rows are for the WR solutions with the smoothness indicator exponent parameter given by $p = R$ (G09; order of accuracy given by $O = 2R - 1$), rather than the traditional value of $p = 2$ (JS96; S97), with rows four, five, and six WR solutions using 100, 66.67, and 50 m. Rows 7–10 are for the WENO solutions with sine wave-based smoothness indicators (WS in left-hand table) made with $p = 1$. Row ten is as in row four for perturbation potential temperature ($T - T_b$; K) for the efficient sine wave-exact WENO-Sine (WS) smoothness indicators and $p = 1$ solution but in the larger sub-domain (compare with Figure 3; notice the absence of anomalous perturbation potential temperature found for the WENO solutions). Maximum (Max) and minimum (Min) values and contour interval (Cint) are on each plot. The bold solid line is the 0.2 K perturbation potential temperature contour of the simulation in the plot. The bold dashed line is the 0.2 K perturbation potential temperature contour of the upwind-biased constant grid flux O17, 25 m reference solution interpolated to the grid in each plot. Only a zoomed-in sub-domain from $x = -5.2$ to -3.6 km and $z = 6.4$ to 7.6 km on the left side of the simulation domain is shown, except in row four through six and the bottom row where a sub-domain is from $x = -6.7$ to -2.7 km and $z = 3.6$ to 7.6 km on the left side of the simulation domain is shown. [Colour figure can be viewed at wileyonlinelibrary.com]



perturbation potential temperatures for $\leq O13$, WR solutions, although there were minor overshoots for the O17, WR solutions as noted above. These higher resolution, WR solutions still had larger RMS errors than found using WENO $p=2$. In addition, the $\geq O13$, 66.67 and 50 m resolution solutions had enhanced shear instabilities on the warm-cold air interface, resulting in small-scale rollups, which were not found in the reference solution. The rollups seemed to be less apparent as resolutions were made finer where diffusion could control them better, and eventually converged to the reference solution, but at finer resolutions than required for WENO solutions made with $p=2$. In summary, the use of $p=R$ in computing WENO fluxes produced potentially both worse and better solutions, which are possible for the complex dynamical problem employed in this article depending on resolution, SGS turbulence, WENO flux order, and the error metrics of most interest. Although the WR solutions were more likely to be monotonic, they had larger RMS errors, and the higher order ($\geq O13$) solutions had more shape differences from anomalous shear instabilities at intermediate resolutions, both of which contributed to the larger RMS errors.

3.4.2 | Accurate and more efficient smoothness indicators for WENO schemes (Set C)

Recently proposed and demonstrated, efficient, sine wave-based WENO smoothness indicators (exact for sine waves; hereafter WS; W20 and W21; note that the coefficients suggested by W21 were recomputed and corrected for this article owing to a couple of typographical errors in W21), for $R \geq 4$ ($\geq O7$) WENO schemes (with comparable order interpolations and pressure gradient/divergence), provided visually better solutions (Figure 14, rows eight–ten, WS; zoomed as in Figures 4–8) for perturbation potential temperature and KE fields, as well as better objective error measure results (Table 3) when compared to solutions with the traditional smoothness indicators for O9, 13 and 17 WENO schemes given by JS96, BS00 and G09. Importantly, the anomalous perturbations in the inner front on top of the lower rotors in the original O13 and O17 WENO solutions are not produced and the maxima and minima are much better behaved with WENO-Sine scheme (compare row five in Figure 3 with row 10 in Figure 14). (Solutions for cases with and without a mean wind for resolutions of 33.33, 66.67, 100 m are provided in Supporting Information S3, and for the nearly full domain, with and without a mean wind, for resolution of 100 m and for with a mean wind for resolutions of 33.33 and 66.67 m are provided in

Supporting information S4.) These newer smoothness indicators required increasingly fewer computations per grid point per time step with each increase in R when compared to traditional WENO schemes of equivalent order as there are three versus R for each stencil for $R \geq 4$. The results herein are in agreement with the findings of W21 who stated that a value for the exponent parameter $p=1$ provided the best solutions with their smoothness indicators. The use of either $p=2$ or $p=R$ (in general >1) with the W21 sine-based smoothness indicators degraded the results for the perturbation potential temperature and KE fields (not shown), as W21 found and explained. These results support the use of the W21 sine-based WENO scheme smoothness indicators for the colliding plumes test problem as formulated as they provided more accurate WENO type solutions using fewer FPOs.

3.4.3 | Lower WENO approximations for stage 1 and 2 of RK3 time integrations (Set D)

One way to reduce the computational cost of implementing very high order advection schemes that are coupled to multi-stage time schemes is to use lower-order flux approximations, for example, in the 1st and 2nd stage calculations of the RK3 time scheme, followed by a very high-order advection scheme for 3rd stage. As an example of the impact of this procedure, Gadd's (1978) multi-dimensional implementation of an O4 advection scheme with a two-step Lax–Wendroff time-integration scheme, used O2 advection for the first Lax–Wendroff “half time step”, followed by O4 advection in the second Lax–Wendroff “half time step”, maintaining the high order accuracy of the O4 advection.

The use of Gadd's approach of computing lower order advection on all but the last stage of a multi-stage time step, was applied herein on the 1st and 2nd stages of RK3/WENO integrations and is shown to be stable and accurate for the combinations considered. Specifically, tests were made for five examples with orders for the RK3 time integration stages one: two: three given by O3:3:17, O5:5:17, O9:9:17, O13:13:17 and O17:17:17 (Figure 15, rows one–three, WL; zoomed as in Figures 4–8). The results from these experiments show that requiring the same high order advection/flux be used for each RK3 stage is not necessary, at least from a practical view, based on perturbation potential temperature and KE fields (Figure 15), and objective error measures (Table 3; compare the values in each column with the values in the last column, as all solutions have O17 for the third stage of the RK3 time integration). Interestingly, the errors were often slightly improved for the most part for the O3:3:17,

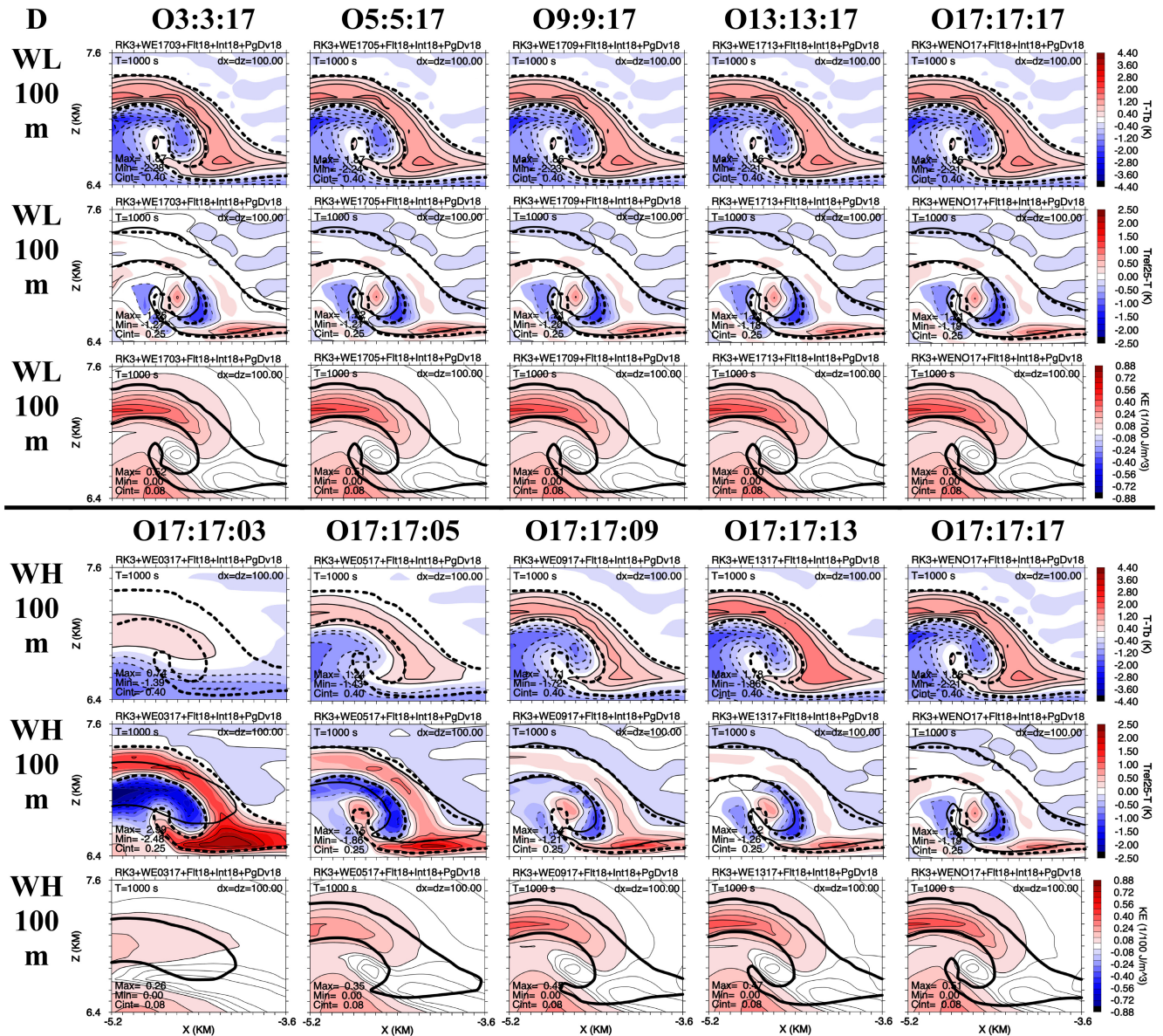


FIGURE 15 Set D perturbation potential temperature ($T - T_b$; K; rows one and four), difference between reference and test solution potential temperature ($T_{\text{ref}} - T$; K; rows two and five), and Kinetic Energy per unit volume (KE ; $1/100 \text{ J} \cdot \text{m}^{-3}$; rows three and six) fields at $t = 1,000 \text{ s}$ made with grid resolution $\Delta x = \Delta z = 100 \text{ m}$, with mixed orders of WENO flux for RK3 time integration stages one, two and three for scalars, velocity and pressure, O18 for all interpolations and pressure gradient/divergence, O18 spatial filter, same Courant number C , and constant eddy mixing coefficient of $K_m = 10 \text{ m}^2 \cdot \text{s}^{-1}$. Rows one – three are WENO flux solutions with orders for RK3 time integrations stages one, two and three given by O3:3:17; O5:5:17; O9:9:17; O13:13:17 and O17:17:17 (WL). Rows four – six are WENO flux solutions with orders for RK3 time integrations stages one, two and three given by O17:17:3; O17:17:5; O17:17:9; O17:17:13 and O17:17:17 (WH). Maximum (Max) and minimum (Min) values and contour interval (Cint) values are on each plot. The bold dashed line is the 0.2 K perturbation potential temperature contour of the upwind-biased constant grid flux O17, 25 m reference solution interpolated to the grid in each plot. The bold solid line is the 0.2 K perturbation potential temperature contour of the simulation in the plot. Only a zoomed-in sub-domain from $x = -5.2$ to -3.6 km and $z = 6.4$ to 7.6 km on the left side of the simulation domain is shown. [Colour figure can be viewed at wileyonlinelibrary.com]

O5:5:17, O9:9:17 WENO solutions compared to using O17 WENO for all three RK3 stages. For the WL results, the order of accuracy of the interpolations and pressure gradient/divergence at each stage were all kept the same as the ones used in the last (third) stage of RK3 time integration; that is, they were all compatible with the highest order

scheme used in the last (third) stage of RK3 time integration, which was O18 for these WL results.

Unsurprisingly, solutions with high order WENO flux for the first two RK3 stages and low order WENO flux for the third stage (i.e. O17:17:3–13; Figure 15, rows four–six, WH solutions; Table 3), only shown for demonstration

purposes, generally did not improve the solutions, when compared to those produced with WL solutions or those with the same order of WENO flux at each RK3 stage. The solutions were made with interpolations and pressure gradient/divergence that were either O18 for all stages (Figure 15 for WL and WH solutions) or the lowest comparable order of accuracy of any of the three stages (not shown; errors provided in Table 3). This demonstration shows that using higher order WENO fluxes, on the 1st and 2nd, than those on the 3rd stage, regardless of the order of accuracy of interpolations and pressure gradient/divergence that were considered, generally did not improve the appearance or objective measures of the WENO solutions. However, solutions for the same order- N WENO fluxes for all three RK3 stages were about the same as using order $<N$ flux on the first two RK3 stages (WL scheme), making the use of WENO potentially much less computationally expensive. Although not tested for other schemes in this article, these results are expected to hold for any of the other schemes besides WENO fluxes considered herein.

3.4.4 | WENO approximations for scalars and constant grid flux for velocity and pressure and vice versa (Set E)

A set of experiments were made using WENO flux only for scalars and constant grid flux for velocity and pressure to determine if these are as accurate as using WENO flux for all variables. While this might not be true for non-viscous problems, especially those with shocks, it might hold for smoother diffusion-limited problems. Both Pressel *et al.* (2015 P15) and WPM21 commented that they did not find degradation of solutions when comparing solutions made with WENO fluxes on only scalars compared to solutions made with WENO fluxes for scalars, velocity and pressure, but neither showed these results as both studies focused on other issues. Both also noted that perhaps the reason for the minimal impact when WENO was not used for velocity fields was that velocity fields tend to be smoother than scalar fields. Simulations with the test problem herein using WENO flux for scalars only (e.g. only potential temperature, but not pressure, which is strongly coupled to velocity for sound waves; arguably, potential temperature is also strongly coupled to velocity for gravity waves through buoyancy), and comparably high order odd order upwind-biased constant grid fluxes for velocity and pressure resulted in perturbation potential temperature and KE fields (Figure 16 rows 1–3 Ws Fv; zoomed as in Figures 4–8; Table 3) that were better objectively than those that used WENO flux for all variables (Table 3). However, the perturbation potential temperature field was

somewhat distorted, although the 0.2 K contour of the potential temperature appeared to capture the upper rotor better. The potential temperature difference fields in the upper rotor were improved, perhaps more for O13–17, when compared to results with WENO flux for all variables in Figure 5.

Simulations with WENO for scalars and constant grid flux for velocity were repeated except using constant grid flux for scalars and WENO flux for velocity and pressure (Figure 16, rows 4–6 Fs Wv; zoomed as in Figures 4–8), which interestingly produced solutions with somewhat worse visual appearances in terms of the shape of 0.2 K contour for potential temperature as well as in some parts of the potential temperature difference fields on the inside and around the base of the upper rotor. In contrast, as in the case for Fv Ws solutions, these Fs Wv solutions also had better objective errors for all solutions for both perturbation potential temperature and KE fields than the solutions with WENO fluxes on all variables (Table 3). The generally reduced objective errors were related to the much better reproduction of the overall amplitude of potential temperature fields compared to the reference solution, even though the L_{\max} and L_{\min} values for KE were not reproduced as well as in the Fv Ws experiments or experiments using WENO for all fluxes. These results were mixed in terms of supporting the use of WENO only for scalar fluxes, or only for velocity and pressure, rather than all fluxes, as objective errors were reduced for some measures, but various aspects of solution appearance were found to be worse for the colliding plumes test problem as formulated.

3.4.5 | Number of derivatives for Crowley schemes (Set F)

Smolarkiewicz (1982) successfully developed dimension-split/time-split 3D and explicit cross-derivative Crowley schemes, which use any order approximation for the advection and O2 approximations for the stabilising second derivatives. Tremback *et al.* (1987), similar to C68, further developed the dimension-split/time-split 3D Crowley schemes by adding stabilising derivatives up to O10 for both odd and even order O1–10 Crowley schemes (N -stabilising derivatives for an N -order scheme). Test simulations made for this article with O3, 5, 9, 13 and 17 Crowley schemes using only the second stabilising derivative ($N = 2$), rather than all N stabilising higher derivatives for N -order Crowley schemes, produced solutions for perturbation potential temperature and KE fields (Figure 17 row one and two, C2; zoomed as in Figures 4–8; Table 3; note the traditional Crowley solutions with N -derivative for an N -order scheme are shown in Figures 3 and 4)

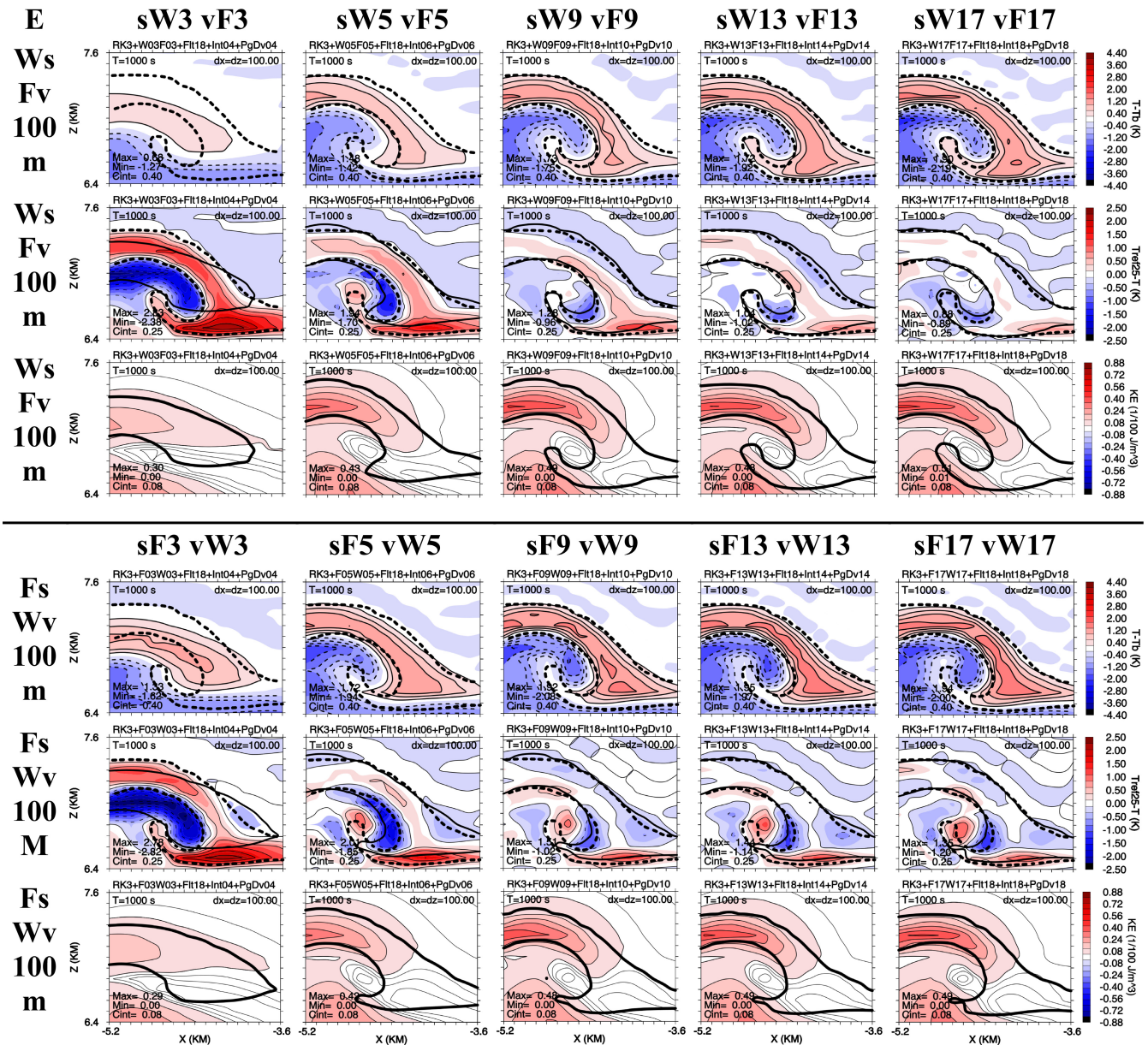


FIGURE 16 Set E perturbation potential temperature ($T - T_b$; K; rows one and four), difference between reference and test solution potential temperature ($T_{\text{Ref}} - T$; K; rows two and five), and Kinetic Energy per unit volume (KE; $1/100 \text{ J} \cdot \text{m}^{-3}$; rows three and six) fields at $t = 1,000 \text{ s}$ made with grid resolution $\Delta x = \Delta z = 100 \text{ m}$, with hybrids of order O3, 5, 9, 13 and 17 WENO flux schemes and comparable odd order upwind-biased constant grid flux, O18 for all interpolations and pressure gradient/divergence, O18 spatial filter, same Courant number C , and constant eddy mixing coefficient of $K_m = 10 \text{ m}^2 \cdot \text{s}^{-1}$. The top three rows are for order O3, 5, 9, 13 and 17 WENO flux for scalars (Ws) and comparable order constant grid flux for velocity and pressure (Fv). The bottom three rows are for O3, 5, 9, 13 and 17 WENO flux for velocity and pressure (Wv) and comparable order constant grid flux for scalars (Fs). Maximum (Max) and minimum (Min) values and contour interval (Cint) values are on each plot. The bold dashed line is the 0.2 K perturbation potential temperature contour of the upwind-biased constant grid flux O17, 25 m reference solution interpolated to the grid in each plot. The bold solid line is the 0.2 K perturbation potential temperature contour of the simulation in the plot. Only a zoomed-in sub-domain from $x = -5.2$ to -3.6 km and $z = 6.4$ to 7.6 km on the left side of the simulation domain is shown. [Colour figure can be viewed at wileyonlinelibrary.com]

that were virtually indistinguishable from each other, both visually and objectively (the schemes with N -higher derivatives were nearly identical or very slightly better objectively for some of the solutions), for any given scheme order. Importantly, these Crowley solutions with $N = 2$

were produced with lower computational costs as only two derivatives were evaluated and not N derivatives. This result can be explained in part by noting that when the Courant number value of $C = u \Delta t \Delta x$ becomes increasingly small (< 1), the values of C^N that are multiplied

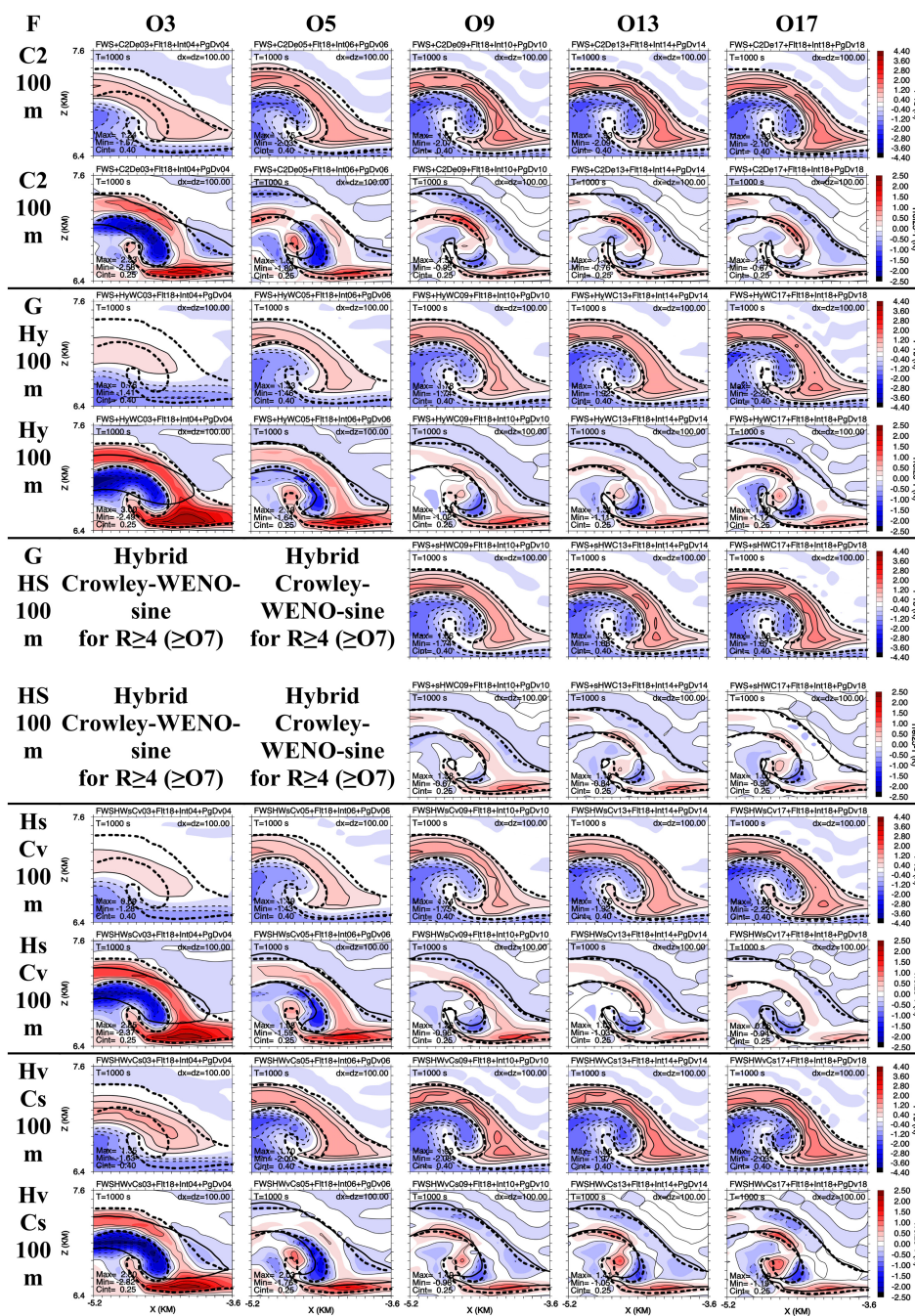


FIGURE 17 Sets F and G Perturbation potential temperature ($T - T_b$; K; rows 1, 3, 5, 7 and 9) and difference between reference and test solution potential temperature ($T_{\text{Ref}} - T$; K; rows 2, 4, 6, 8 and 10) at $t = 1,000$ s made with grid resolution $\Delta x = \Delta z = 100$ m, with odd order O3, 5, 9, 13 and 17 upwind-biased constant grid flux Crowley and hybrid-WENO/Crowley schemes, comparable order interpolations and pressure gradient/divergence, O18 spatial filter, same Courant number C , and constant eddy mixing coefficient of $K_m = 10 \text{ m}^2 \cdot \text{s}^{-1}$. The top two rows are for upwind-biased odd order O3, 5, 9, 13 and 17 constant grid flux Crowley scheme using only the stabilizing second derivative (C2), rather than N derivatives for an N -th order scheme. Rows three and four are for hybrid-WENO/Crowley (Hy) flux schemes (Set G in rows three and four and all remaining rows). Rows five and six are for hybrid-WENO/Crowley flux schemes made with sine wave-based WENO-s smoothness indicators and $p = 1$ (HS). Rows seven and eight are for hybrid-WENO/Crowley flux schemes for scalars (Hs) and Crowley for velocity and pressure (Cv). Rows nine and ten for hybrid-WENO/Crowley fluxes on velocities and pressure (Hv) and Crowley on scalars (Cs). Maximum (Max) and minimum (Min) values and contour interval (Cint) values are on each plot. The bold dashed line is the 0.2 K perturbation potential temperature contour of the upwind-biased constant grid flux O17, 25 m reference solution interpolated to the grid in each plot. The bold solid line is the 0.2 K perturbation potential temperature contour of the simulation in the plot. Only a zoomed-in sub-domain from $x = -5.2$ to -3.6 km and $z = 6.4$ to 7.6 km on the left side of the simulation domain is shown. [Colour figure can be viewed at wileyonlinelibrary.com]

with each N -th derivative become increasingly small and less impactful (e.g. with a Courant number value used in this study of $C = 0.046875$, values for $C^2 \sim 2.197 \times 10^{-3}$, $C^3 \sim 1.03 \times 10^{-4}$, ..., $C^9 \sim 1.09 \times 10^{-12}$, $C^{17} \sim 2.547 \times 10^{-23}$, etc.), than if $C = 0.9$ ($C^2 = 0.81$, $C^3 = 0.729$, ..., $C^9 \sim 0.3874$, $C^{17} \sim 0.1668$, etc.). The Crowley simulations shown all use the difference-stencils (related to order of accuracy) for the higher order derivatives suggested by T87, noting that the order accuracy for the approximations for lower derivatives are generally higher order, but the highest order derivatives in T87 are not the order of the higher order derivatives (presumably this practice is not a serious issue as at least the even order derivatives are dissipative). Rather the approximations are the highest order of accuracy that will fit in the length of the stencil used to compute the interpolation for the first derivative. Note that comparable order interpolations and pressure gradient/divergence were used for all Set E simulations. In summary, these results support the use of only the second stabilising derivative, as objective and visual appearances were not changed and solutions were computationally less expensive than using N derivatives for an N -order Crowley scheme.

3.4.6 | Hybrid-WENO/Crowley schemes (Set G)

Dimension-split/time-split hybrid-WENO/Crowley schemes were tested as the use of higher order derivatives sometimes can help reduce phase errors (e.g. T87; WS02). Furthermore, the WS02 forward-in-time Crowley scheme time integration procedure for mode-split systems with only one(two) functions per time step for scalars (velocities and pressure) is notably less computationally intensive in terms of total FPOs for any given order of flux using the spatial differencing algorithm discussed in Section 2, compared to the RK3 time integration scheme, which requires three functions per time step for scalars, velocities and pressure, respectively. With this in mind, the use of WENO fluxes in a Crowley scheme framework might be advantageous computationally as well as numerically. Experiments were conducted with a proposed hybrid-WENO/Crowley scheme, which has interpolation for the flux obtained from the WENO scheme, and upwind-biased constant grid flux higher order derivatives. Comparable order interpolations and pressure gradient/divergence were used for all Set G simulations.

Visually accurate perturbation potential temperature and KE solutions were obtained with the Hybrid-WENO-Crowley schemes (Hy) when compared to the WENO and odd order Crowley solutions in Set A (e.g. Figure 4). The potential temperature perturbation

difference plots (Figure 17, row four) showed patterns and regions of errors for Hybrid-WENO-Crowley that were more similar to those with the Set A, WENO solutions than the Set A, odd order Crowley solutions (Figure 5). Objective errors, including RMS for perturbation potential temperature and KE (Table 3) for the Hybrid-WENO-Crowley schemes were similar to those with the WENO schemes for these simulations. Additionally, like with the WENO scheme, the Hybrid-WENO-Crowley scheme and sine-based WENO smoothness indicator scheme, also produced improved perturbation potential temperature difference fields from the reference solution and improved RMS errors, based on the reference solution, over those made with traditional smoothness indicators by $\sim 5\%$ to $\geq 20\%$, especially for the O17 solutions. These results are important as the computational cost based on FPOs of the forward in time Hybrid-WENO-Crowley schemes, for either traditional or sine-based smoothness indicators, are markedly less than RK3 WENO solutions, especially for higher order solutions.

Using hybrid-WENO/Crowley flux for scalars and Crowley flux on velocities and pressure also performed well (Figure 17, rows seven and eight, Hs Cv; zoomed as in Figures 4–8; Table 3), while the use of hybrid-WENO/Crowley on velocities and pressure only and Crowley flux on scalars produced better results for perturbation potential temperature (Figure 17, rows nine and ten, Hv Cs; zoomed as in Figures 4–8; Table 3) and KE fields (not shown), than using WENO on all variables, both with further reductions in computational cost from the cases of using WENO fluxes on all variables (the differences were again somewhat worse than for odd order Crowley). Although not shown, comparably accurate solutions, which were virtually indistinguishable, either visually (not shown) or objectively (Table 3; H2S) were also possible using only the stabilising second derivative and no other higher order stabilising derivatives in these hybrid schemes. In summary, computational costs can be reduced, and objective errors notably improved using hybrid-WENO/Crowley schemes with or without the sine-based smoothness indicators, as well as with or without stabilising higher order derivative or only the stabilising second derivative. Additionally, use of hybrid WENO/Crowley fluxes on either scalars or velocities and pressure, especially for the hybrid-WENO on velocities and pressure and Crowley on scalars (Hs Cv) might help provide more accurate solutions than using WENO flux on all variables; the HsCv and HvCs solutions appeared visually better compared to the WENO solutions, but visually not as good as the Crowley solutions. This appeared to be the case for the objective errors as well.

3.4.7 | Use of lower order approximations for velocity and pressure advection and higher order for scalars and vice versa (Set H)

Finally, a set of simulations was made to determine whether higher order accuracy flux of velocities and pressure or higher order flux of scalars (potential

temperature) was more important to solution accuracy, while potentially allowing for some reduced computational costs. Pressel *et al.* (2015) and WPM21 both stated that the velocity fields are generally smoother than the scalar fields in their atmospheric planetary boundary layer simulations (which was also seen with KE fields herein), and thus did not require velocity flux schemes to be as

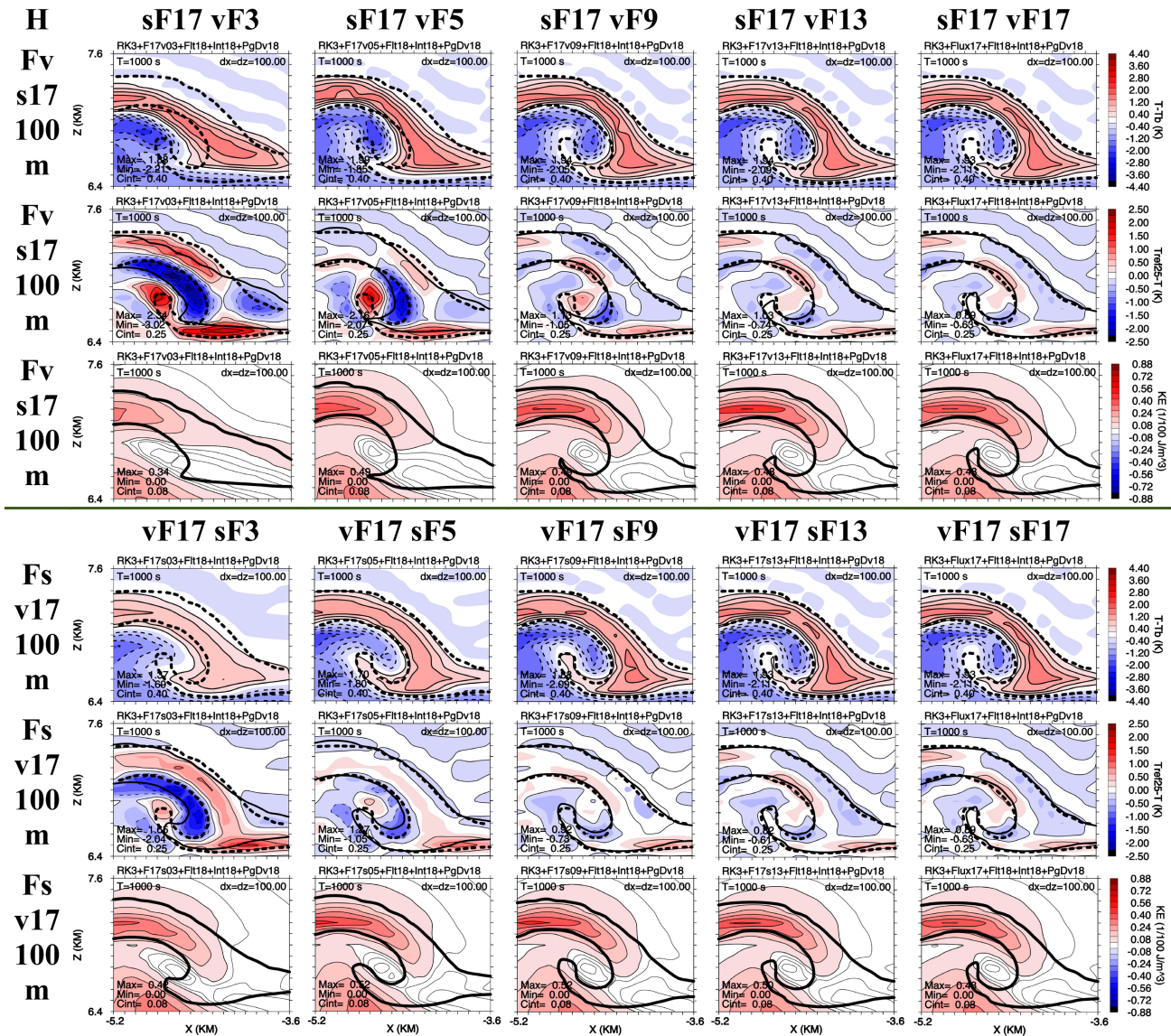


FIGURE 18 Set H perturbation potential temperature ($T - T_b$; K; rows one and four), difference between reference and test solution potential temperature ($T_{\text{Ref}} - T$; K; rows two and five), and Kinetic Energy per unit volume (KE; $1/100 \text{ J} \cdot \text{m}^{-3}$; rows three and six) fields at $t = 1,000 \text{ s}$ made with grid resolution $\Delta x = \Delta z = 100 \text{ m}$, with O3, 5, 9, 13 and 17 upwind-wind biased constant grid flux schemes, all with O18 interpolations and pressure gradient/divergence, O18 spatial filter, same Courant number C , and eddy mixing coefficient of $K_m = 10 \text{ m}^2 \cdot \text{s}^{-1}$. The top three rows are for odd order O3, 5, 9, 13 and 17 constant grid flux schemes for velocity and pressure (Fv) and the O17 constant grid flux scheme for scalars (s17). The second three rows are for odd order O3, 5, 9, 13 and 17 constant grid flux schemes for scalars (Fs) and the odd order O17 constant grid flux scheme for velocity and pressure (v17). Maximum (Max) and minimum (Min) values and contour interval (Cint) values are on each plot. The bold dashed line is the 0.2 K perturbation potential temperature contour of the upwind-biased constant grid flux O17, 25 m reference solution interpolated to the grid in each plot. The bold solid line is the 0.2 K perturbation potential temperature contour of the simulation in the plot. Only a zoomed-in sub-domain from $x = -5.2$ to -3.6 km and $z = 6.4$ to 7.6 km on the left side of the simulation domain is shown. [Colour figure can be viewed at [wileyonlinelibrary.com](#)]

accurate as scalar flux schemes. The simulations shown herein include those made with O17 fluxes for scalars and O3–17 fluxes for velocities and pressure, and well as those made using O17 fluxes for velocities and pressure, and O3–17 fluxes for scalars. These were used to compare with simulations using O17 fluxes for all variables (Figures 3 and 4–8). All Set H simulations (Figure 18) used O(18) interpolations and pressure gradient/divergence.

The amplitudes of the perturbation potential temperature fields in the most marginally resolved features of the upper rotor for the first subset of experiments were best preserved with O17 scalar fluxes, although the shape is not as well preserved (as compared to the Set A odd order flux solutions in Figure 4 or the reference solution) in association with less accurate velocity and pressure fluxes (Figure 18, rows one–three, Fv s17; zoomed as in Figures 4–8; Table 3). In addition, the 0.2 K perturbation potential temperature contour was not as well preserved compared to the Set A solutions or the reference solution. Conversely, the second subset of experiments produced worse amplitude preservation of the perturbation potential temperature fields with O3–13 scalar fluxes, compared to the reference solution, but about the same as in Set A, with slightly better placement and shape for the rotor associated with O17 velocities (Figure 18, rows 4–6 Fs v17; zoomed as in Figures 4–8; Table 3). Interestingly, the use of lower order fluxes with scalars rather than velocity and pressure resulted in generally better objective error measures than Set A odd order flux solutions and better 0.2 K perturbation potential temperature contour preservation in the upper rotor, especially in the narrow warm regions for most solutions, owing to lower order scalar fluxes being more dispersive, which makes the >0.2 K regions wider, especially in finer scale regions of the upper rotor. The perturbation potential temperature difference fields also had smaller differences when using lower order (O3–5) scalar fluxes. These characteristics permit gross determinations as to which of these subsets of experiments produce the best solutions for all orders considering competing factors. The best solutions in these experiments were the Fs v17 solutions based on RMS errors for potential temperature and KE, as well as for perturbation potential temperature field differences, especially for O3–9 solutions.

4 | CONCLUSIONS

The main conclusions of this study include: The visual appearances and objective error measures for solutions produced by all schemes considered continued to improve well through flux orders of O3/4–9/10, which are the highest orders available/used in most popular research and

operational 3D atmospheric science numerical models, and all the way up to O17/18. Most of the visual and objective improvements were from O3 to O5, and then from O5 to O9, and so on, although they often were not negligible from O13–17. Higher order numerical approximations also improved the accuracy of kinematic aspects of flows as seen using quantities such as KE, deformation and vorticity. Upwind-biased, odd order, very high order flux schemes produced the least dispersion/phase errors with only minimally damped extrema at very high orders of accuracy $>O13$ when compared to the reference solution. Very high order even order $\geq O14$ schemes, which better preserve amplitude errors over one order lower odd schemes and have slightly worse phase errors than one order higher odd schemes, also performed very well. Excessive round-off error accumulation argues against using much higher than O17/18 constant grid flux and constant grid flux Crowley schemes, and especially against using higher than O13 or O17 WENO flux schemes.

The WENO flux schemes did not perform as well as the constant grid flux and constant grid flux Crowley schemes for O3–9 solutions made with resolutions coarser than 50 m, supporting the results described by Latini *et al.* (2006) and WPM21 that $\leq O5$ WENO solutions could be excessively dissipative. Interestingly, the very high order O9–17 WENO flux scheme solutions made with a strong added mean wind were the most accurate for a given resolution, with some of the lowest overall objective errors, in this study. Importantly, the $\leq O13$ WENO flux solutions also tended to be more monotonic at intermediate and coarser solutions, in contrast to other schemes, even though WENO scheme solutions are technically not monotonic. While WENO schemes certainly were much more computationally expensive than most schemes considered in terms of FPOs, they were not necessarily excessively/prohibitively expensive with careful use of cache memory in making computations; the CPU time for O17 WENO was at most three to four times more than the CPU time O17 flux.

Only weak numerical spatial filters were generally needed with odd order high order constant grid flux and constant grid flux Crowley schemes in contrast to even-order schemes, which required much more filtering for low orders of accuracy as they tend to produce more dispersion and aliasing errors. Very high order constant grid flux non-WENO schemes, which had appropriate spatial filters for the diffusion-limited problem, produce solutions that were comparable or better than both lower order and higher order WENO based solutions at a fraction of the cost in terms of FPOs or CPU time, especially the forward in time WS02 Crowley based flux solutions.

The WENO flux solutions made with the exponent parameter $p = R$ in the nonlinear weights for WENO fluxes were generally less accurate based on RMS errors than those using the traditional value of $p = 2$ for the test problem. Using by $p = R$ improved maximum and minimum perturbation potential temperature overshoots and generally helped maintain more monotonic WENO flux solutions, although shear instabilities formed in these WENO solutions on the warm-cold air interface at coarser resolutions of greater than 50 m with higher order $>O13$ WENO schemes, that was not present in the reference solution. Importantly, the use of recently proposed, efficient and fewer (three versus R for each stencil; for $R \geq 4$) sine-wave WENO smoothness indicators, which are exact for sine waves, along with $p = 1$, produced solutions that were in good agreement with the reference solution, and were more accurate than solutions made with traditional WENO smoothness indicators. Using less than order N WENO flux for the first two stages of the three RK3 stages of order N WENO solutions produced solutions that were as accurate as using order N WENO flux advection on all three RK3 stages, especially if the WENO flux order for the first two stages is not very small (e.g. $O3$) compared to the last stage (e.g. $O17$). Other findings include that, solutions made with odd order constant grid flux for velocities and pressure and WENO flux for scalars, were better solutions than those made with odd order constant grid flux for scalars and WENO flux for velocities and pressure, and both were more accurate, especially the former, evaluated against the reference solution as compared to the use of WENO flux advection for all variables. The anti-WENO (A-WENO) $O3$ and $O5$ flux schemes proposed by WPM21 to improve the excessive smoothing by lower order WENO schemes might be considered for improvement of high order WENO schemes, but the A-WENO approach might not be necessary with higher order ($\geq O7$) WENO or other flux schemes. Finally, the adaptive order WENO flux schemes based on Legendre polynomials, which result in much simpler smoothness indicator approximations (Balsara *et al.*, 2009, 2016), as well as the use of hybrid-WENO flux schemes, which only use nonlinear WENO fluxes in regions of steep gradients or approximate discontinuities with efficient high order flux schemes in smoother flow regions (Hu *et al.*, 2015) should be explored for atmospheric problems. These schemes seem very attractive as most regions in atmospheric flows are rather smooth compared to non-viscous gas dynamics flows. The proposed hybrid-WENO flux scheme is promising as WENO flux is only applied at a small number of grid points ($<1\%$) and requires only a simple numerical test to determine whether the WENO flux should replace the more efficient high order flux.

A proposed dimension-split hybrid-WENO/Crowley advection scheme integrated in time with the WS02 two-step Crowley forward-in-time integration scheme, which allowed for fast/slow mode-split time integration, produced accurate solutions with fewer FPOs compared with either traditional or newer efficient smoothness indicators, with $p = 2$ for the traditional, or $p = 1$ for the newer smoothness indicators, respectively. This was true for hybrid-WENO/Crowley flux scheme used for all scalars, velocity and pressure, or with hybrid-WENO/Crowley flux scheme for only scalars and constant grid flux Crowley for velocity and pressure.

Crowley scheme solutions made with just the stabilising $O2$ spatial derivatives, compared to those with N higher order derivatives for an N th order scheme, produced nearly identical solutions and lowered the number of FPOs. This also was true for the hybrid-WENO/Crowley flux scheme. Use of lower order odd order constant grid flux for scalars, and high order odd order constant grid flux for velocities produced better solutions in terms of the shape of the flow field features, but worse amplitudes of the potential temperature compared to the reference solution in the marginally resolved regions, than the use of the high order odd order constant grid flux for velocity and pressure, and lower order odd constant grid flux for scalars. Finally, the mode-split time integration solutions produced with constant grid flux Crowley schemes were the least computationally expensive of all schemes considered in terms of either FPOs or CPU in this study for any given order of accuracy and resolution owing largely to being amenable to being written in a condensed form. Otherwise, they would have been more computationally expensive than the constant grid flux RK3 integrations, as was found by WS02.

Future assessments of very high order numerical schemes should be made using realistic atmospheric forecast problems, especially those that require high accuracy, have complex physics, and can be integrated for relatively long periods of time relative to their spatial scales. Examples of problems that might be considered are those related to significant weather forecast for hail, winds, and tornadoes with severe storms, extreme winds and precipitation with hurricanes, heavy snow with lake effect and synoptic systems, as well as a multitude of short-term climate problems associated with excess precipitation, heat and drought, and cold waves.

In summation, upwind-biased, very high order ($O9$ – $O18$) flux schemes performed very well in the experiments described in this article, especially the non-WENO flux schemes, although the high order WENO flux schemes produced very good solutions in experiments

with a strong mean wind. The odd order schemes, which generally require less spatial filtering (WENO flux schemes technically required none) compared to the lower order even schemes that were considered, were only slightly more computationally expensive (two function evaluations are required for odd order schemes for each step or sub-step), when compared to even order centred flux schemes. Objective error measures for non-WENO flux schemes improved to O17/18, while those for WENO flux schemes did not improve much past O9 or O13 for intermediate resolutions of ≥ 50 m. The use of high order flux computations coupled with high order interpolation and pressure gradient/divergence numerical approximations ($\geq O4$) are recommended to attain the best solutions, especially for physically important, marginally resolved phenomena, as was found for short-term integrations presented in this article. The results of this study lead us to encourage the further testing of very high order $\geq O9$ flux schemes in numerical weather prediction and weather research models.

AUTHOR CONTRIBUTIONS

Jerry M. Straka: Conceptualization; data curation; formal analysis; investigation; methodology; project administration; resources; software; validation; visualization; writing – original draft; writing – review and editing. **Katharine M. Kanak:** Conceptualization, formal analysis; investigation; visualization; writing – review and editing. **Paul D. Williams:** Conceptualization; investigation; writing – review and editing.

ACKNOWLEDGEMENTS

The authors thank the reviewers for their very useful comments, recommendations, and insights. The first author is grateful to G. Gerolymos, B. Fornberg and C.-W. Shu for very promptly answering many questions about high order schemes over the past several years.

FUNDING INFORMATION

There are no funding statements to report.




CONFLICT OF INTEREST

There are no conflicts of interest disclosure, ethics approval statement, patient consent statement, permissions to reproduce material from other sources, or clinical trial registration, to report.

DATA AVAILABILITY STATEMENT

The source codes and input files are available from the authors.

ORCID

Jerry M. Straka  <https://orcid.org/0000-0003-3672-5858>
Katharine M. Kanak  <https://orcid.org/0000-0003-3479-9669>
Paul D. Williams  <https://orcid.org/0000-0002-9713-9820>

REFERENCES

- Asselin, R. (1972) Frequency filter for time integrations. *Monthly Weather Review*, 100, 487–490. [https://doi.org/10.1175/1520-0493\(1972\)100<0487:FFFTI>2.3.CO;2](https://doi.org/10.1175/1520-0493(1972)100<0487:FFFTI>2.3.CO;2).
- Baldauf, M. (2008) Stability analysis for linear discretisations of the advection equation with Runge–Kutta time integration. *Journal of Computational Physics*, 227(13), 6638–6659. <https://doi.org/10.1016/j.jcp.2008.03.025>.
- Baldauf, M. (2010) Linear stability analysis of Runge–Kutta-based partial time-splitting schemes for the Euler equations. *Monthly Weather Review*, 138(12), 4475–4496. <https://doi.org/10.1175/2010MWR3355.1>.
- Balsara, D.S., Garain, S. and Shu, C.-W. (2016) An efficient class of WENO schemes with adaptive order. *Journal of Computational Physics*, 326, 780–804. <https://doi.org/10.1016/j.jcp.2016.09.009>.
- Balsara, D.S., Rumpf, T., Dumbser, M. and Munz, C.-D. (2009) Efficient, high accuracy ADER-WENO schemes for hydrodynamics and divergence-free magnetohydrodynamics. *Journal of Computational Physics*, 228(7), 2480–2516. <https://doi.org/10.1016/j.jcp.2008.12.003>.
- Balsara, D.S. and Shu, C.-W. (2000) Monotonicity preserving weighted essentially non-oscillatory schemes with increasingly high order of accuracy. *Journal of Computational Physics*, 160, 405–452.
- Borges, R., Carmona, M., Costa, B. and Don, W.S. (2008) An improved weighted essentially non-oscillatory scheme for hyperbolic conservation laws. *Journal of Computational Physics*, 227, 3191–3211. <https://doi.org/10.1016/j.jcp.2007.11.038>.
- Bott, A. (1989) A positive definite advection scheme obtained by non-linear renormalization of the advective fluxes. *Monthly Weather Review*, 117, 1006–1015.
- Bryan, G.H. (2021) The governing equations for CM1. *UCAR Tech. Note*, 30 https://www2.mmm.ucar.edu/people/bryan/cm1/cm1_equations.pdf.
- Bryan, G.H. and Fritsch, J.M. (2002) A benchmark simulation for moist nonhydrostatic numerical models. *Monthly Weather Review*, 130(12), 2917–2928. [https://doi.org/10.1175/1520-0493\(2002\)130<2917:ABSFMN>2.0.CO;2](https://doi.org/10.1175/1520-0493(2002)130<2917:ABSFMN>2.0.CO;2).
- Castro, M., Costa, B. and Don, W.S. (2011) High order weighted essentially non-oscillatory WENO-Z schemes for hyperbolic conservation Laws. *Journal of Computational Physics*, 230, 1766–1792.
- Clappier, A. (1998) A correction method for use in multidimensional time-splitting advection algorithms: application to two- and three-dimensional transport. *Monthly Weather Review*, 126, 232–242.
- Costa, A.A. and Sempio, A.J.C. (1997) Bott's area-preserving flux-form advection algorithm: extension to higher orders and additional tests. *Monthly Weather Review*, 125, 1983–1989.

- Crowley, W.P. (1968) Numerical advection experiments. *Monthly Weather Review*, 96, 1–11. [https://doi.org/10.1175/1520-0493\(1968\)096<0001:NAE>2.0.CO;2](https://doi.org/10.1175/1520-0493(1968)096<0001:NAE>2.0.CO;2).
- Durran, D.R. (2010) *Numerical Methods for Fluid Dynamics*, Second edition. New York: Springer-Verlag.
- Easter, R.C. (1993) Two modified versions of Bott's positive definite numerical advection scheme. *Monthly Weather Review*, 121, 297–304.
- Fjortoft, R. (1953) On the changes in spectral distribution of kinetic energy for two dimensional nondivergent flow. *Tellus*, 5, 225–230. <https://doi.org/10.3402/tellusa.v5i3.8647>.
- Fornberg, B. (1987) The pseudospectral method: comparisons with finite differences for the elastic wave equation. *Geophysics*, 52, 483–501.
- Fornberg, B. (1988) Generation of finite difference formulas on arbitrarily spaced grids. *Mathematics of Computation*, 51, 699–706.
- Gadd, A.J. (1978) A numerical advection scheme with small phase speed errors. *Quarterly Journal of the Royal Meteorological Society*, 104, 583–594.
- Gerolymos, G.A., Sénéchal, D. and Vallet, I. (2009) Very-high-order WENO schemes. *Journal of Computational Physics*, 228, 8481–8524.
- Grabowski, W.W. and Clark, T.L. (1991) Cloud–environment interface instability: rising thermal calculations in two spatial dimensions. *Journal of the Atmospheric Sciences*, 48(4), 527–546. [https://doi.org/10.1175/1520-0469\(1991\)048<0527:CIHTC>2.0.CO;2](https://doi.org/10.1175/1520-0469(1991)048<0527:CIHTC>2.0.CO;2).
- Haltiner, G.J. and Williams, R.T. (1980) *Numerical Prediction and Dynamical Meteorology*. New York: John Wiley and Sons, Inc., p. 477 ISBN 0-471-05971-4.
- Hu, X., Wang, B. and Adams, N.A. (2015) An efficient low-dissipation hybrid weighted essentially non-oscillatory scheme. *Journal of Computational Physics*, 301, 415–424.
- Jiang, G.-S. and Shu, C.-W. (1996) Efficient implementation of weighted ENO schemes. *Journal of Computational Physics*, 126, 202–228.
- Knievel, J.C., Bryan, G.H. and Hacker, J.P. (2007) Klemp, J.B. and Wilhelmson, R.B. (1978) The simulation of three-dimensional convective storm dynamics. *Journal of the Atmospheric Sciences*, 35(6), 1070–1096. [https://doi.org/10.1175/1520-0469\(1978\)035<1070:TSOTDC>2.0.CO;2](https://doi.org/10.1175/1520-0469(1978)035<1070:TSOTDC>2.0.CO;2).
- Latini, M., Schilling, O. and Don, W. (2006) *Effects of WENO Flux Reconstruction Order and Spatial Resolution on Reshocked Two-Dimensional Richtmyer-Meshkov Instability*. Livermore, CA: Lawrence Livermore National Laboratory UCRL-TR-220015.
- Leonard, B.P. (1991) The ULTIMATE conservative difference scheme applied to unsteady one-dimensional advection. *Computational Methods in Applied Mechanics and Engineering*, 88, 17–74.
- Lian, Y., Richardson, M.I., Newman, C.E., Lee, C., Toigo, A., Guzewich, S. and Yelle, R.V. (2023) Dynamical core damping of thermal tides in the Martian atmosphere. *Journal of the Atmospheric Sciences*, 80, 535–547.
- Lunet, T., Christine, L., Auguste, F., Visentin, F., Masson, V. and Escobar, J. (2017) Combination of WENO and explicit Runge–Kutta methods for wind transport in the Meso-NH model. *Monthly Weather Review*, 145, 3817–3838. https://doi.org/10.1175/MWR-D-16_0343.1.
- Morrison, H. and Bryan, G.H. (2012) Sensitivity of a simulated squall line to horizontal resolution and parameterization of microphysics. *Monthly Weather Review*, 140, 202–225. <https://doi.org/10.1175/MWR-D-11-00046.1>.
- Norman, M.R. (2021) A high-order WENO-limited finite-volume algorithm for atmospheric flow using the ADER-differential transform time discretization. *Quarterly Journal of the Royal Meteorological Society*, 147, 1661–1690. <https://doi.org/10.1002/qj.3989>.
- Park, S.-H. and Lee, T.-Y. (2009) High-order time-integration schemes with explicit time-splitting methods. *Monthly Weather Review*, 137, 4047–4060. <https://doi.org/10.1175/2009MWR2885‐1>.
- Pressel, K.G., Kaul, C.M., Schneider, T., Tan, Z. and Mishra, S. (2015) Large-eddy simulation in an anelastic framework with closed water and entropy balances. *Journal of Advances in Modeling Earth Systems*, 7, 1425–1456. <https://doi.org/10.1002/2015MS000496>.
- Purser, R.J. (1987) The filtering of meteorological fields. *Journal of climate and Applied Meteorology*, 26(12), 1764–1769. [https://doi.org/10.1175/1520-0450\(1987\)026<1764:TFOMF>2.0.CO;2](https://doi.org/10.1175/1520-0450(1987)026<1764:TFOMF>2.0.CO;2).
- Purser, R.J. (2007) Accuracy considerations of time-splitting methods for models using two-time-levels schemes. *Monthly Weather Review*, 135(3), 1158–1164. <https://doi.org/10.1175/MWR3339.1>.
- Purser, R.J. and Leslie, L.M. (1988) A semi-implicit, semi-Lagrangian finite difference scheme using high-order spatial differences on a nonstaggered grid. *Monthly Weather Review*, 116, 2069–2080.
- Qiu, J. and Shu, C.-W. (2002) On the construction, comparison, and local characteristic decomposition for high-order central WENO schemes. *Journal of Computational Physics*, 183, 187–209. <https://doi.org/10.1006/jcph.2002.7191>.
- Schlesinger, R.E. (1984) Mature thunderstorm cloud top structure and dynamics: a three-dimensional numerical simulation study. *Journal of the Atmospheric Sciences*, 41, 1551–1570.
- Schlesinger, R.E. (1985) Effects of upstream-biased third-order space correction terms on multidimensional Crowley advection schemes. *Monthly Weather Review*, 113(7), 1109–1130. [https://doi.org/10.1175/1520-0493\(1985\)113<1109:EOUBTO>2.0.CO;2](https://doi.org/10.1175/1520-0493(1985)113<1109:EOUBTO>2.0.CO;2).
- Shapiro, R. (1970) Smoothing, filtering, and boundary effects. *Reviews of Geophysics*, 8(2), 359–387. <https://doi.org/10.1029/RG008i002p00359>.
- Shi, J., Zhang, Y.-T. and Shu, C.-W. (2003) High order WENO schemes for complicated flow structures. *Journal of Computational Physics*, 186, 690–696.
- Shu, C.-W. (1988) Total-variation-diminishing time discretizations. *SIAM Journal on Scientific Computing*, 9, 12, 1073–1084. <https://doi.org/10.1137/0909073>.
- Shu, C.-W. (1997) Essentially non-oscillatory and weighted essentially non-oscillatory schemes for hyperbolic conservation laws. NASA/CR-97-206253 ICASE Report No. 97-65. 79 pp.
- Shu, C.-W. (2003) High-order finite difference and finite volume WENO schemes and discontinuous Galerkin methods for CFD. *International Journal of Computational Fluid Dynamics*, 17, 107–118. <https://doi.org/10.1080/1061856031000104851>.
- Shu, C.-W. and Osher, S. (1988) Efficient implementation of essentially non-oscillatory shock-capturing schemes. *Journal of Computational Physics*, 77, 439–471. [https://doi.org/10.1016/0021-9991\(88\)90177-5](https://doi.org/10.1016/0021-9991(88)90177-5).
- Shuman, F.G. (1957) Numerical methods in weather prediction. II: smoothing and filtering. *Monthly Weather Review*,

- 85(11), 357–361. [https://doi.org/10.1175/1520-0493\(1957\)085<0357:NMIWPI>2.0.CO;2](https://doi.org/10.1175/1520-0493(1957)085<0357:NMIWPI>2.0.CO;2).
- Skamarock, W.C. and Klemp, J.B. (1992) The stability of time-split numerical methods for the hydrostatic and the nonhydrostatic elastic equations. *Monthly Weather Review*, 120(9), 2109–2127. [https://doi.org/10.1175/1520-0493\(1992\)120<2109:TSOTSN>2.0.CO;2](https://doi.org/10.1175/1520-0493(1992)120<2109:TSOTSN>2.0.CO;2).
- Smolarkiewicz, P.K. (1982) The multi-dimensional Crowley advection scheme. *Monthly Weather Review*, 110(12), 1968–1983. [https://doi.org/10.1175/1520-0493\(1982\)110<1968:TMDCAS>2.0.CO;2](https://doi.org/10.1175/1520-0493(1982)110<1968:TMDCAS>2.0.CO;2).
- Smolarkiewicz, P.K. (1985) On the accuracy of the Crowley advection scheme. *Monthly Weather Review*, 113(8), 1425–1429. [https://doi.org/10.1175/1520-0493\(1985\)113<1425:OTAOTC>2.0.CO;2](https://doi.org/10.1175/1520-0493(1985)113<1425:OTAOTC>2.0.CO;2).
- Soong, S.-T. and Ogura, Y. (1973) A comparison between axisymmetric and slab-symmetric cumulus models. *Journal of the Atmospheric Sciences*, 30, 879–893.
- Straka, J.M. and Anderson, J.R. (1993) Extension and application of a local, minimum aliasing method to multidimensional problems in limited-area domains. *Monthly Weather Review*, 121, 2903–2918. [https://doi.org/10.1175/1520-0493\(1993\)121<2903:EAAOAL>2.0.CO;2](https://doi.org/10.1175/1520-0493(1993)121<2903:EAAOAL>2.0.CO;2).
- Straka, J.M., Wilhelmson, R.B., Wicker, L.J., Anderson, J.R. and Droegemeier, K.K. (1993) Numerical solutions of a non-linear density current: a benchmark solution and comparisons. *International Journal for Numerical Methods in Fluids*, 17(1), 1–22. <https://doi.org/10.1002/fld.1650170103>.
- Straka, J.M., Williams, P.D. and Kanak, K.M. (2023) Nonlinear diffusion-limited 2D colliding plume simulations with very high order O3–17 flux, O2–18 interpolation, O2–18 pressure gradient/divergence, and O2–10 turbulent flux numerical approximations. Revision submitted to Quarterly Journal of the Royal Meteorological Society.
- Tan, K.-A., Morison, R. and Leslie, L.M. (2005) A comparison of high-order explicit and non-oscillatory finite difference advection schemes for climate and weather models. *Meteorology and Atmospheric Physics*, 89, 251–267. <https://doi.org/10.1007/s00703-005-0132-0>.
- Tremback, C.J., Powell, J., Cotton, W.R. and Pielke, R.A. (1987) The forward-in-time upstream advection scheme: extension to higher orders. *Monthly Weather Review*, 115(2), 540–555. [https://doi.org/10.1175/1520-0493\(1987\)115<0540:TFTUAS>2.0.CO;2](https://doi.org/10.1175/1520-0493(1987)115<0540:TFTUAS>2.0.CO;2).
- Walko, R.L. and Avissar, R. (2008) The ocean–land–atmosphere model (OLAM). Part II: formulation and tests of the non-hydrostatic dynamic core. *Monthly Weather Review*, 136(11), 4045–4062. <https://doi.org/10.1175/2008MWR2523.1>.
- Wang, A., Pan, Y. and Markowski, P.M. (2021) The influence of WENO schemes on large-eddy simulations of a neutral atmospheric boundary layer. *Journal of the Atmospheric Sciences*, 78(11), 3613–3628. <https://doi.org/10.1175/JAS-D–21-0033.1>.
- Wicker, L.J. (2009) A two-step adams-bashforth-moulton split-explicit integrator for compressible atmospheric models. *Monthly Weather Review*, 137, 10, 3588–3595. <https://doi.org/10.1175/2009MWR2838.1>.
- Wicker, L.J. and Skamarock, W.C. (2002) Time-splitting methods for elastic models using forward time schemes. *Monthly Weather Review*, 130(8), 2088–2097. [https://doi.org/10.1175/1520-0493\(2002\)130<2088:TSMFEM>2.0.CO;2](https://doi.org/10.1175/1520-0493(2002)130<2088:TSMFEM>2.0.CO;2).
- Williams, P.D. (2009) A proposed modification to the Robert–Asselin time filter. *Monthly Weather Review*, 137, 2538–2546. <https://doi.org/10.1175/2009MWR2724.1>.
- Williams, P.D. (2011) The RAW filter: an improvement to the Robert–Asselin filter in semi-implicit integrations. *Monthly Weather Review*, 139, 1996–2007. <https://doi.org/10.1175/2010MWR3601.1>.
- Williams, P.D. (2013) Achieving seventh-order amplitude accuracy in leapfrog integrations. *Monthly Weather Review*, 141(9), 3037–3051. <https://doi.org/10.1175/MWR-D–12-00303.1>.
- Williams, P.D., Straka, J.M. and Kanak, K.M. (2022) The performance of filtered leapfrog schemes in benchmark simulations. *Quarterly Journal of the Royal Meteorological Society*, 148, 784–808. <https://doi.org/10.1002/qj.4231>.
- Williamson, J.H. (1980) Low storage Runge-Kutta schemes. *Journal of Computational Physics*, 35, 48–56.
- Wu, C., Wu, L., Li, H. and Zhang, S. (2021) Very high order WENO schemes using efficient smoothness indicators. *Journal of Computational Physics*, 432, 110158.
- Wu, C., Wu, L. and Zhang, S. (2020) A smoothness indicator constant for sine functions. *Journal of Computational Physics*, 419, 109661. <https://doi.org/10.1016/j.jcp.2020.109661s>.
- Zhang, Y.T., Shi, J., Shu, C.W. and Zhou, Y. (2003) Numerical viscosity and resolution of high-order weighted essentially nonoscillatory schemes for compressible flows with high Reynolds numbers. *Physical Review E*, 68, 046709. <https://doi.org/10.1103/PhysRevE.68.046709>.

SUPPORTING INFORMATION

Additional supporting information can be found online in the Supporting Information section at the end of this article.

How to cite this article: Straka, J.M., Kanak, K.M. & Williams, P.D. (2023) Comparison of very high order (O3–18) flux and Crowley flux, and (O3–17) WENO flux schemes with a 2D nonlinear test problem. *Quarterly Journal of the Royal Meteorological Society*, 149(757), 3669–3710. Available from: <https://doi.org/10.1002/qj.4579>

APPENDIX A

TABLE A1 CFL and critical wave number at which instability appears first based for O1–19 linear odd order upwind biased (by one point) advection schemes with WSO2 O3 Runge–Kutta (LRK3) time integration using and extending the procedures described by Baldauf (2008).

LRK3 ODD	O1	O3	O5	O7	O9	O11	O13	O15	O17	O19
CFL	1.256373	1.625891	1.434983	1.243779	1.127174	1.049315	0.9935351	0.9514629	0.9184809	0.8918446
Kcrit	3.141593	2.472898	1.693186	1.763554	1.847447	1.922732	1.988061	2.044338	2.093085	2.135942

TABLE A2 CFL and critical wave number at which instability appears first based for O2–20 linear even order centred advection schemes with WSO2 O3 Runge–Kutta (LRK3) time integration using and extending the procedures described by Baldauf (2008).

LRK3 EVEN	O2	O4	O6	O8	O10	O12	O14	O16	O18	O20
CFL	1.732051	1.262224	1.092102	1.000839	0.942644	0.901712	0.8710421	0.8470229	0.8275891	0.8114673
Kcrit	1.570796	1.797478	1.936074	2.033371	2.107086	2.165720	2.213967	2.254671	2.289680	2.320252

TABLE A3 CFL at which instability appears first based for O2–20 linear even order centred advection with (LLF) time integration to compare to LRK3.

LLF EVEN	O2	O4	O6	O8	O10	O12	O14	O16	O18	O20
CFL	1.0	0.7287451	0.6305261	0.5778348	0.5442359	0.5206038	0.5028964	0.4890290	0.4778089	0.4685009

Note: As can be shown, the CFLs for O2–20 linear even order centred advection schemes with WSO2 O3 Runge–Kutta time integrations (see Table A2) are always ~1.732051 more than the same order advection and leapfrog time integrations.

APPENDIX B

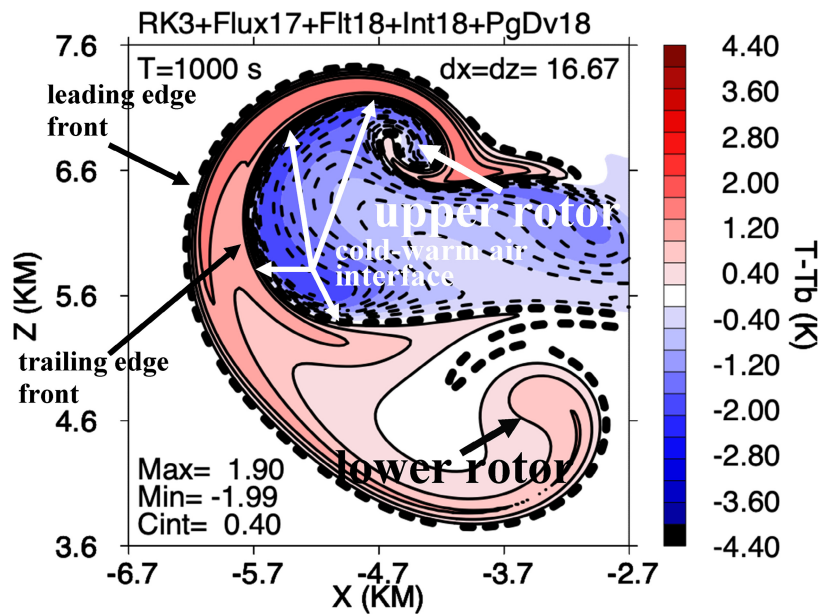


FIGURE B Locations of flow structures in the perturbation potential temperature field for the colliding plumes circulation in a solution made with O17 constant grid fluxes, O18 interpolations and pressure gradient/divergence, O18 spatial filter, and constant eddy mixing coefficient of $K_m = 10 \text{ m}^2 \cdot \text{s}^{-1}$ using $\Delta x = \Delta z = 16.66 \dots \text{m}$ and $\Delta t = 0.0520833 \dots$ (adapted from SWK23). [Colour figure can be viewed at wileyonlinelibrary.com]